8-2019

Provenance and Maximum Depositional Age Analysis of the Moenave Formation using Detrital Zircon U-Pb Geochronology and Sandstone Petrography

Asher Rea Boudreaux
University of Arkansas, Fayetteville

Provenance and Maximum Depositional Age Analysis of the Moenave Formation using Detrital Zircon U-Pb Geochronology and Sandstone Petrography

A thesis submitted in partial fulfillment
of the requirements for the degree of
Master of Science in Geology

by

Asher Boudreaux
University of Arkansas
Bachelor of Science in Geology, 2017

August 2019
University of Arkansas

This thesis is approved for recommendation to the Graduate Council.

Glenn Sharman, Ph.D.
Thesis Director

Celina Suarez, Ph.D.
Committee Member

Barry Shaulis, Ph.D.
Committee Member

Abstract

In southwestern Utah and northeastern Arizona, Moenave Formation (latest Triassic(?)-Jurassic) is bracketed by well-studied Mesozoic units extensively sampled for detrital zircon geochronology and is poorly documented in regard to provenance, representing an important gap in knowledge. The Moenave Formation provides a unique opportunity to employ detrital zircon U-Pb geochronology and sandstone petrography relevant to completing the paleogeographic, evolutionary, and climatic story of the region. This study aims to characterize the sedimentary provenance of the Moenave Formation and to identify, or at least improve constraints on, the stratigraphic position of the Triassic-Jurassic boundary (TJB) and placement of the end-Triassic extinction (ETE), if present at all, within the Moenave Formation. The present work (1) expands the database of detrital zircon data for the Moenave Formation with U-Pb ages from 5190 individual detrital zircon analyses from 22 samples collected from three study sites and (2) adds petrographic analyses using 400 modal point counts per thin section for 26 samples. This study reports individual and composite U-Pb age distributions and provenance ternary diagrams of the Moenave Formation and surrounding units, as well as apply nine different maximum depositional age (MDA) calculations from the resulting detrital zircon data. Comparison of composite U-Pb age distributions and petrographic detrital modes show strong similarities in sediment dispersal and composition between the Moenave and Kayenta formations. The age distribution of the Moenave Formation consists of dominant age peaks that indicate the Moenave Formation was derived from a number of sources including the Cordilleran arc, Appalachian Orogeny, Grenville Orogeny, Mesoproterozoic plutons, and Yavapai-Mazatzal sources. Conservative MDA estimates (YC2σ, Y3Zo, YSP, and the τ method) are consistent with a stratigraphic placement of the ETE

within the lower DCM. These results are in agreement with existing provenance and chemostratigraphic interpretations regarding the stratigraphic location of the ETE.

Acknowledgments

Field work on the Navajo Nation was conducted under a permit from the Navajo Nation Minerals Department. Any persons wishing to conduct geologic investigations on the Navajo Nation must first apply for and receive a permit from the Navajo Nation Minerals Department, P.O. Box 1910, Window Rock, Arizona. Fieldwork in Zion National Park was conducted under permit ZION-2018-SCI-0001. Thanks to Dr. Adam Marsh and Benn Breeden for help with sampling, Spectrum Petrographics for creating the thin sections for this study, Erik Pollock for help with LA-ICP-MS issues, and Jordan Oefinger for help measuring the Blacks Canyon stratigraphic section. I would also like to thank my committee members, Dr. Glenn Sharman, Dr. Celina Suarez, and Dr. Barry Shaulis for their guidance and patience. Furthermore, I would like to thank my parents, Rea and Sharon Boudreaux, my fiancée, Lauren Butcher, and my friend, Tanner Corbin, for their continued support throughout graduate school at the University of Arkansas. This material is based upon work supported by the National Science Foundation under Grant No. 1761576.

Table of Contents

Chapter 1: Introduction

Popularity in using detrital zircon geochronology has grown rapidly within geoscience research over the past two decades due to the versatile information that can be obtained from U-Pb isotopic measurements and the ability to integrate this data with other geochemical, sedimentologic, biostratigraphic, magnetostratigraphic, and geochronologic information (Gehrels, 2014). Although, there have been multiple studies that have conducted detrital zircon analyses of Mesozoic units within the region of southwestern Utah and northern Arizona, this area still provides a unique opportunity to employ this methodology within the Moenave Formation. Stratigraphically bracketed by the well-studied underlying Chinle Formation (Riggs et al., 1996; Dickinson et al., 2008; Marsh et al., 2019) and overlying Kayenta Formation (Dickinson et al., 2009a; Marsh, 2019), the Moenave Formation represents an important gap in knowledge relevant to completing the paleogeographic, evolutionary, and climatic story of the region.

The purpose of this research is to use combined detrital zircon U-Pb geochronology and sandstone petrography to characterize the sedimentary provenance of the Moenave Formation and to improve constraints on its depositional age. As the lowest member of the Glen Canyon Group, the Moenave Formation is composed of latest Triassic(?) to earliest Jurassic fluvio-lacustrine deposits that crop out in southwestern Utah to northeastern Arizona (Tanner and Lucas, 2007; Milner et al., 2012; Kirkland et al., 2014; Suarez et al., 2017). Although the underlying Chinle Formation and overlying Kayenta Formation have been extensively sampled for detrital zircon geochronology via chemical abrasion (CA-ID-TIMS) and laser ablation (e.g., Dickinson et al., 2008; 2009a; Marsh et al., 2019), the provenance of the Moenave Formation is poorly documented with only two known published samples from Suarez et al. (2017) with a limited sample size (93 grain analyses in total). This preliminary data suggested that the Moenave Formation may have a

distinct detrital zircon U-Pb age spectra relative to surrounding stratigraphic units (Suarez et al., 2017). Here, the present work (1) expands the database of detrital zircon data for the Moenave Formation with U-Pb ages from 5190 individual detrital zircon analyses from 22 samples collected from three study sites and (2) adds petrographic analyses using 400 modal point counts per thin section for 26 samples. This study reports individual and composite U-Pb age distributions and provenance ternary diagrams of the Moenave Formation and surrounding units. Detrital zircon U-Pb age distributions show the Moenave age spectrum consists of multiple age populations of Mesozoic Cordilleran arc ages (50-300 Ma), Appalachian and peri-Gondwanan ages (300-800 Ma), Grenvillian ages (800-1300 Ma), Mesoproterozoic pluton ages (1300-1550 Ma), Yavapai-Mazatzal ages (1550-1800Ma) and North Laurentia ages (greater than 1800 Ma) (Fig. 1). Comparison of composite U-Pb age distributions and petrographic detrital modes show strong similarities between the Moenave and Kayenta formations. Sediment dispersal pathways originated from the south (the Mogollan Slope and Appalachian/ Grenville derived sources) and southwest (the Cordilleran magmatic arc) of the Colorado Plateau and from adjacent erg deposits.

Furthermore, this study aims to identify, or at least improve constraints on, the stratigraphic position of the TJB (201.3 ± 0.2 Ma.; Hillebrandt et al., 2013) and the end-Triassic extinction (201.564 ± 0.015 Ma.; Blackburn et al., 2013) within the Moenave Formation. The Moenave Formation has been hypothesized to contain the ETE (Suarez et al., 2017), a significant climatic and biotic event that has been linked with the release of volcanic CO_2 into the atmosphere from the Central Atlantic Magmatic Province (Marzoli et al., 1999). The stratigraphic position of the TJB and ETE, if present at all, is controversial (Milner et al., 2012; Kirkland et al., 2014). Previous methods using stratigraphic context and correlation, biostratigraphy, magnetostratigraphy, chemostratigraphy, and radiogenic dating have all been employed within the Moenave Formation

to identify the TJB and ETE (Donohoo-Hurley et al., 2010; Lucas et al., 2011; Milner et al., 2012; Kirkland et al., 2014; Suarez et al., 2017; Antonietto et al., 2018). This work extends the list of methods to aid in in the clarity of the TJB and ETE stratigraphic positions by applying nine different maximum depositional age calculations from detrital zircon U-Pb laser ablation data using methods outlined by Coutts et al. (2019). Using an aggregate of conservative MDA calculations within each study section help constrain the ETE within the lower DCM. The sedimentary record in southwestern Utah contains an abundant fossil record; the added constraints on the stratigraphic placement of the ETE provide clarification to the age of the Moenave Formation, which helps the regional paleontological community in deciphering the age of fossils and paleoecological change across the boundary.

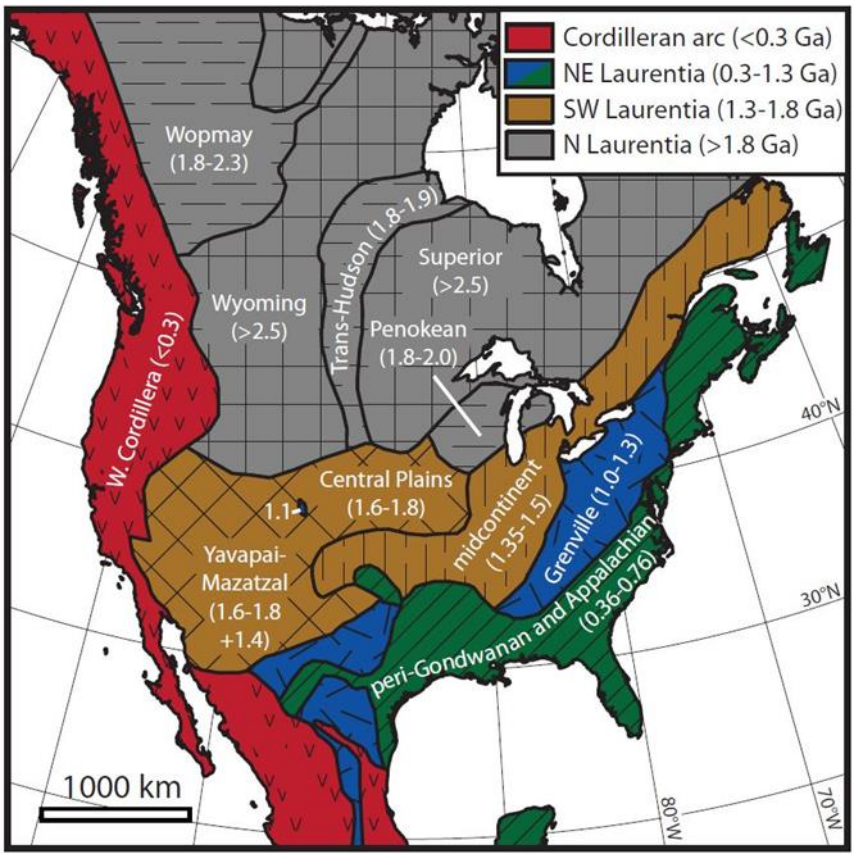

Figure 1: Map of North American basement provinces and their crystallization age (Ga). Modified from Dickinson and Gehrels (2009), Fildani et al. (2016), and Sharman et al. (2018).

Chapter 2: Geologic Background

Geologic Setting

The study area is located within southwestern Utah and northeastern Arizona and within the Colorado Plateau (Fig. 2; Fig. 3). The Moenave Formation is the lowest member of the Glen Canyon Group and is late Triassic (Rhaetian) to Early Jurassic (Hettangian) in age (~202-196 Ma) (Tanner and Lucas, 2009; Milner et al., 2012; Kirkland et al., 2014; Suarez et al., 2017). The Moenave Formation comprises a succession of continental redbeds, averaging 100 m in thickness that includes sandstone, siltstone, and mudstone deposited by fluvial, lacustrine, and eolian processes (Harshbarger et al., 1957; Clemmensen et al., 1989; Tanner and Lucas, 2007), and consists of two members, the Dinosaur Canyon Member (DCM) and the Whitmore Point Member (WPM). The Moenave Formation is stratigraphically positioned between the underlying Chinle Formation at the J-0 unconformity, and the overlying Springdale Sandstone of the Kayenta Formation at the J-0' unconformity (Pipiringos and O'Sullivan, 1978; Marzolf, 1993; Kirkland et al., 2014). Sediments were deposited in a retro-arc basin, regionally known as the Zuni sag, that formed on the western edge of the North American craton as a result of collision with the Cordilleran magmatic arc system (Blakey, 1994; Dickinson, 2009). The Zuni sag was a depression across the southern Colorado Plateau during deposition of the Glen Canyon Group and was a locus of northwesterly flowing streams (Riggs and Blakey, 1993). Previous interpretations of the source area for these sediments was mainly the Mogollon slope, located approximately 500 km to the south and southwest (Tanner and Lucas, 2009; Fig. 2).

Dinosaur Canyon Member (DCM)

The DCM is an extensive northwest trending fluvial to lacustrine system with interfingering eolian deposits (Fig. 2A; Harshbarger et al., 1957; Kirkland et al., 2014). It is

composed of reddish, quartz-rich, fine to very fine sandstones with interbedded mudstones. The basal unit of the DCM is marked by a conglomeratic interval containing chert and anhydrite pebbles (Kirkland et al., 2014). Most sandstone units contain abundant planar bedding, climbing ripples, and trough crossbedding suggesting a high flux of sediment was deposited at a relatively rapid rate (Tanner and Lucas, 2007; Suarez et al., 2017). Fluvial sandstones within the DCM were deposited mainly by channel aggradation by different ephemeral stream processes indicated by three types of sandstone-body architectures: sandstone-sheets interbedded with mudstones interpreted as sheet flood deposits; simple channel sandstone-bodies interpreted as solitary incised channel deposits; and multi-story channel sandstone-bodies interpreted as braided stream deposits (Olsen, 1989). Evidence of sandstones deposited by eolian processes are found along the margin of the Wingate erg located east and south of the Moenave Formation outcrop belt. The Wingate Sandstone is an erg deposit that consists of large-scale, cross-stratified, fine-grained sandstones formed by migrating dunes and is considered to be equivalent to the Moenave Formation (Clemmensen et al., 1989; Tanner and Lucas, 2007). At the erg margin the Wingate Sandstone and the DCM interfinger where fluvial and eolian sandstones are deposited. This can be explained by controlling factors to erg-margin dynamics including climate variations in aridity and humidity (Clemmensen et al., 1989). During arid intervals, ephemeral braided streams transported sandy bedload into the erg-margin area, where eolian reworking took place. During humid intervals, sheet-floods and high-sinuosity rivers transported a more mud-rich sediment load into the basin, where eolian activity was minimal (Clemmensen et al., 1989). Following a span of erosion, when significant portions of the Triassic Chinle Formation were removed, the J-0 unconformity marks a period of uplift near the southwest margin of the Colorado Plateau, followed by a gentle northwest regional tilt. DCM ephemeral streams flowed northwestward along the Zuni sag and

were confined between the Wingate erg complex to the northeast and the Mogollon slope to the southwest (Riggs and Blakey, 1993; Blakey, 1994; Fig. 2).

Whitmore Point Member (WPM)

The WPM represents an extensive shallow lacustrine environment that formed either due to increased precipitation in the Zuni sag basin, increased subsidence of the northern Zuni sag, or both (Fig. 2B; Kirkland et al., 2014). WPM strata were deposited on the terminal floodplain of the Moenave DCM alluvial system in a large, laterally extensive, shallow lake system with fluctuating water levels (Tanner and Lucas, 2009; Kirkland et al., 2014). The WPM is composed of shales, siltstones, sandstones, and minor limestones, and can be divided into three intervals: a lower shale and sandstone interval, a middle sandstone interval, and an upper shale interval. The lower shale dominated interval is highly fossiliferous and is interpreted to be a distal lacustrine environment (Kirkland et al, 2014; Suarez et al., 2017). The middle sandstone interval contains invertebrate burrows and dinosaur tracks and is interpreted as a migrating sandbar (Kirkland et al, 2014; Suarez et al., 2017). The upper shale dominated interval is also fossiliferous and includes trace fossils and dinosaur tracks. This interval is interpreted to oscillate between distal and proximal lacustrine environments (Kirkland et al, 2014; Suarez et al., 2017).

Study Sites

Study sites for this research are located along the Moenave Formation outcrop belt (Fig. 3) at Olsen Canyon within Warner Valley near St. George, Utah (37.0181°, -113.3893°); Blacks Canyon within Zion National Park, Utah (37.1991°, -113.0014°); and Willow Springs near Tuba City, Arizona (36.1751°,-111.3862°). A description of the Olsen Canyon section and Blacks Canyon section was provided by Suarez et al. (2017). A description of the Willow Springs section was provided by Marsh (2019).

Chronology

In the absence of ammonites and other marine invertebrates, other age-relevant criteria have been used to date the Moenave Formation (Milner et al., 2012; Kirkland et al., 2014). Previous attempts to determine the placement of the TJB and ETE of the Moenave Formation were based upon stratigraphic context and correlation, vertebrate biostratigraphy, palynology, paleomagnetism, carbon isotope chemostratigraphy, and limited detrital zircon geochronology (Downs, 2009; Tanner and Lucas, 2009; Donohoo-Hurley et al., 2010; Lucas et al., 2011; Milner et al., 2012; Kirkland et al., 2014; Steiner, 2014; Suarez et al., 2017).

No tetrapod taxa, skeletal remains or tracks from Triassic-age strata have been found in the Moenave Formation. Instead, all of the tetrapod data identified so far are consistent with being post-ETE, which could be very latest Triassic or Early Jurassic (Milner et al., 2012; Kirkland et al., 2014). *Grallator* dominated trackways that lack *Eubrontes* can be found within lower DCM strata. The laterally equivalent Wingate Sandstone contains upper Triassic tetrapod fauna (*Redondasaurus*) and ichnofauna (*Brachychirotherium)* that are exclusively pre-ETE, but still not found in the Moenave, and phytosaurs, which are exclusively pre-ETE. This evidence suggests a late Triassic age for the lower part of both formations (Tanner and Lucas, 2009). Three ichnotaxa, *Eubrontes, Anomoepus, Bratrachopus,* known only from post-ETE strata globally, first appear near the middle of the DCM. The lowest occurrence of *Eubrontes* is approximately 17.2 meters above the J-0 unconformity. This suggests the ETE, if present, is in the lower DCM. (Olsen et al., 2002; Kirkland et al., 2014; Suarez et al., 2017). Downs (2009) described palynomorph assemblages from the lower DCM of the Moenave Formation and concluded that there were examples of the otherwise pre-ETE *Patinasporites* and *Vallasporites* from the lower half of the DCM. This suggests that the ETE lies within the lower DCM. Milner et al. (2012) argues that the

rare *Patinasporites* are poorly preserved and suggests the occurrence of these assemblages be further documented. Thus, based on biostratigraphic evidence, the ETE can be loosely constrained within the lower DCM and Wingate sandstone (Tanner and Lucas, 2009; Downs, 2009; Milner et al., 2012; Kirkland et al., 2014; Suarez et al., 2017).

Donohoo-Hurley et al. (2010) incorporated magnetostratigraphic methods within the Moenave Formation at four locations, encompassing southwestern Utah and northern Arizona, and correlated the results with equivalent formations across the globe. Donohoo-Hurley et al. (2010) placed the TJB based on their magnetostratigraphic interpretations approximately 3 to 13 meters above the DCM-WPM contact within the WPM. Lucas et al. (2011) built upon the magnetostratigraphic data from Donohoo-Hurley et al. (2010) and expanded the results of the previous work with supporting biostratigraphy data, stating that *Eubrontes* and *Grallator* are only preserved in the lower WPM about 4 meters above the DCM-WPM contact. Both studies concluded that the TJB must have occurred within the lower to middle WPM. However, these studies fail to mention the *Eubrontes* and *Grallator* occurrence in the upper 8 meters of the DCM at the Saint George Dinosaur Discovery Site at Johnson Farm (Milner et al., 2012). Furthermore, the biostratigraphic and magnetostratigraphic levels in eastern North America and England to which these studies refer, lie within the latest Rhaetian strata (Kirkland et al., 2014). Steiner (2014) incorporated magnetostratigraphy methods within the WPM and found that the WPM strata exhibited a dominant normal geomagnetic polarity. In comparison to other basins, Steiner (2014) concluded that the WPM section most resembled the fossiliferous Hettangian strata of the Paris Basin which suggests that the WPM is Hettangian in age.

Carbon isotope chemostratigraphy of ETE sections globally show a distinct negative carbon isotope excursion that is related to the eruption of the Central Atlantic Magmatic Province,

a large igneous province that likely spurred on rapid climate change, habitat degradation, and biotic crisis associated with the ETE (Blackburn et al., 2013; Guex et al., 2014; Hesselbo et al., 2002; Marzoli et al., 1999; Schaller et al., 2015; Schoene et al., 2010; Whiteside et al., 2010). The ETE was estimated by Blackburn et al. (2013) at 201.564 ± 0.015 Ma. Suarez et al. (2017) used carbon isotope chemostratigraphy and detrital zircon data to support the claims that the TJB if present, should be within the middle to upper DCM, or lower WPM, while the ETE, associated with the Central Atlantic Magmatic Province, if present, should be within the lower to middle DCM. Two TIMS ages were determined from detrital zircons of 201.33 ± 0.07/0.12 Ma (Suarez et al., 2017) from the upper sands of the DCM at Potter Canyon, Arizona and 201.28 ± 0.11/0.15 Ma (Suarez et al., 2017) from the middle sandstone of the WPM at Blacks Canyon, Utah. A significant negative C-isotope excursion was found at the base of the WPM near the sampled detrital zircons. This excursion, however, does not correlate with the initial negative carbon isotope excursion at the ETE, but rather post-dates the ETE in accordance with the detrital zircon ages (Suarez et al., 2017). This also changes the previous interpretations of Donohoo-Hurley et al. (2010) and Lucas et al. (2011) by placing the ETE and the TJB stratigraphically lower in the Moenave.

Detrital Zircon U-Pb Geochronology

The underlying Chinle Formation (Late Triassic) and overlying Kayenta Formation (Early Jurassic) have been extensively sampled for detrital zircon geochronology (e.g., Riggs et al., 1996; Dickinson and Gehrels, 2008; 2009a). During deposition of the Chinle-Dockum Group, a through-going river system connected Texas with the Cordilleran continental margin across the Colorado Plateau indicating that early during Late Triassic time, the continental interior was topographically low (Riggs et al., 1996). Provenance studies from detrital zircons indicate three master paleodrainage courses, flowing from southeast to northwest, were active during the fluvial

systems' evolution (Riggs et al., 1996; Dickinson and Gehrels, 2008). The three paleodrainage courses were, the Eagle paleoriver, the principal lower Chinle-Dockum trunk paleoriver, and the upper Chinle-Dockum Cottonwood paleovalley (Dickinson and Gehrels, 2008). The Eagle paleoriver had its headwaters near the Amarillo-Wichita uplift and was dominated by Cambrian grains. The lower and upper Chinle-Dockum paleodrainage systems derived sediment from the Ouachita orogen, the Permian-Triassic East Mexico arc and the Cordilleran arc which was increasingly more prominent during Late Triassic time (Dickinson and Gehrels, 2008). The lower Chinle-Dockum paleodrainage system represents the depositional environment for the regional Chinle Formation relative to this study's sample locations.

Most detrital zircon grains in Jurassic eolianites, including the Wingate Sandstone, were derived ultimately from basement provinces older than 285 Ma in eastern and central Laurentia, rather than from rock assemblages of the nearby Cordilleran margin (Dickinson and Gehrels, 2009a). The lower Jurassic fluvial Springdale Sandstone is the basal member of the Kayenta Formation stratigraphically located above the Moenave Formation. Provenance analyses suggest that Springdale streams mixed detritus from Yavapai-Mazatzal basement of southwest Laurentia with arc-derived Cordilleran detritus without contributions from the East Mexico arc. This is distinctly different from the rest of the Kayenta Formation with sediment derived from an admixture of redistributed eolian sand and younger arc detritus (Dickinson and Gehrels, 2009a).

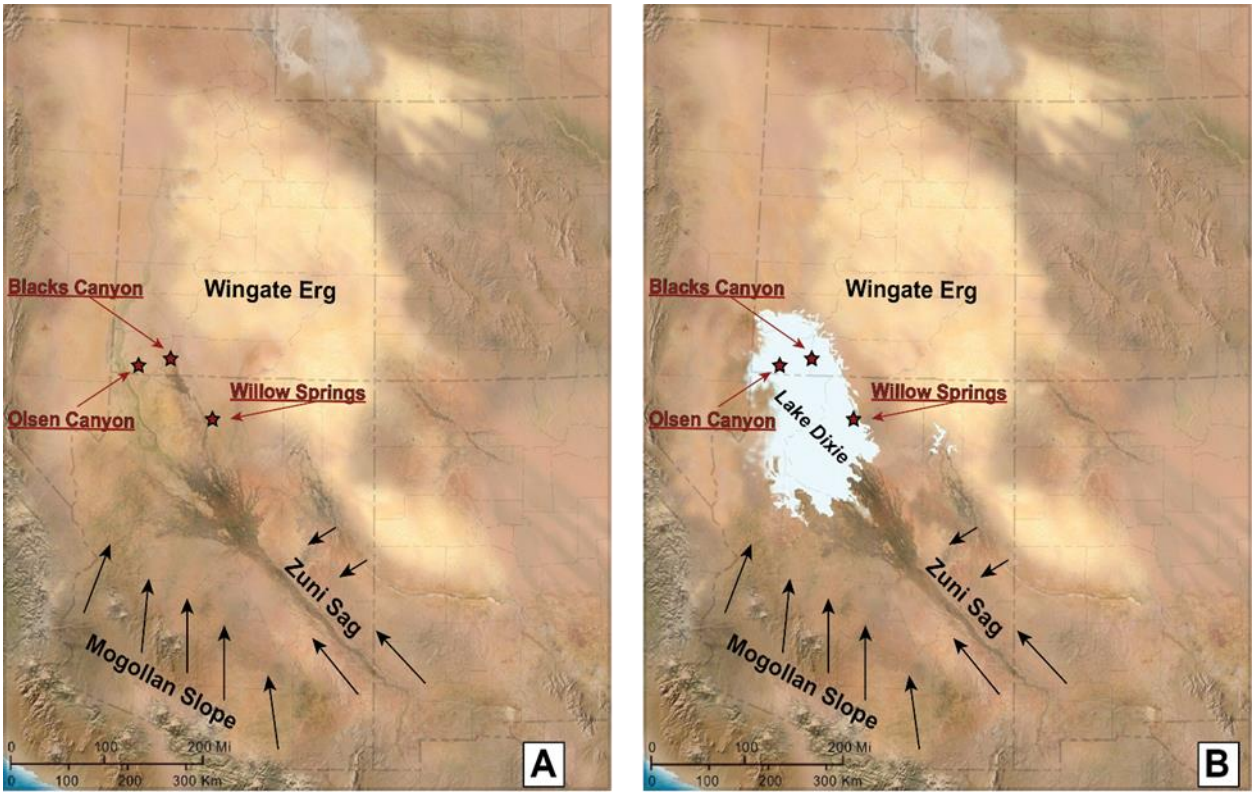

Figure 2: Paleogeographic map during time of deposition. Black arrows indicate fluvial transport pathways. Study sites are located with red stars. **A:** The Dinosaur Canyon Member during time of deposition, showing river systems flowing from the southeast toward the northwest along the Zuni sag, between the Wingate erg and the Mogollan Slope. **B:** The Whitmore Point Member during time of deposition, showing the estimated maximum extent of Lake Dixie

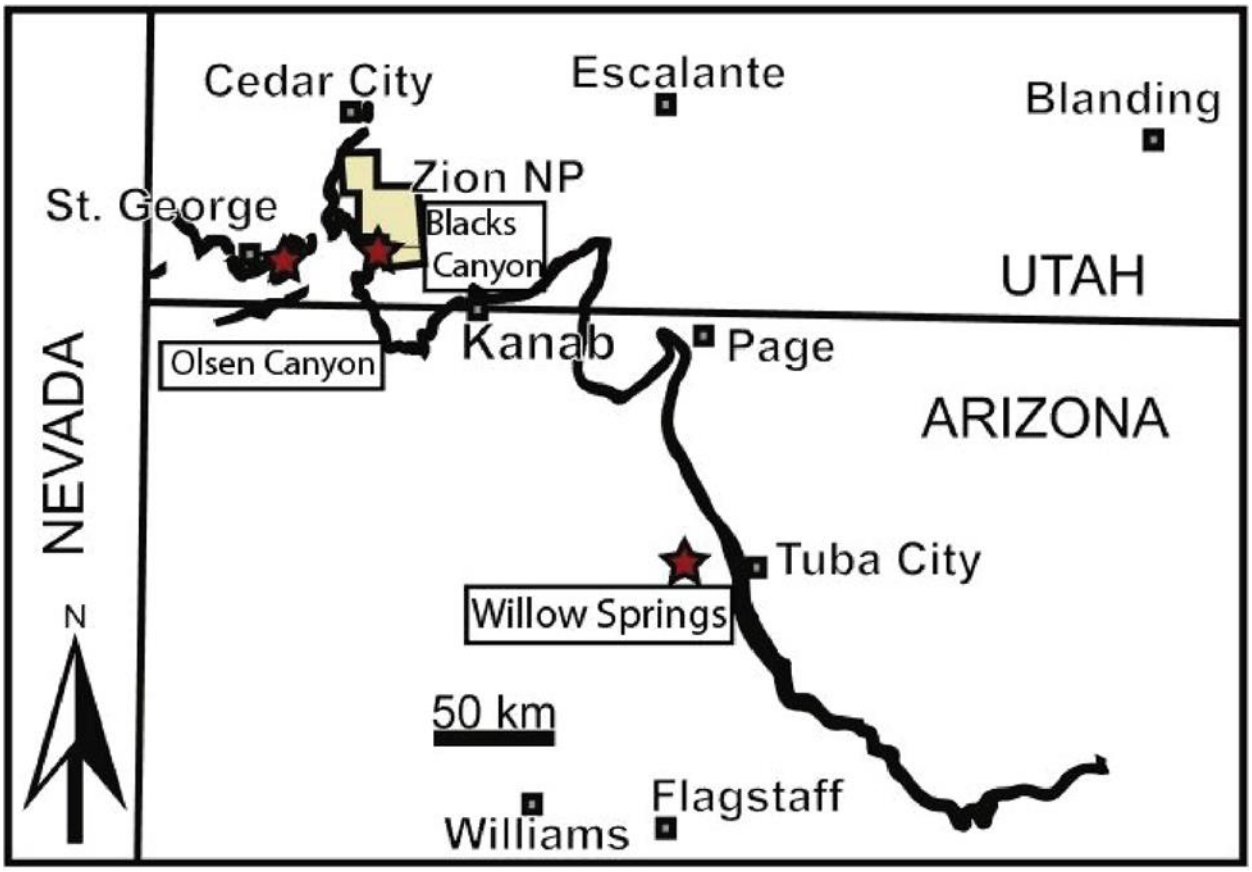

Figure 3: Map of Moenave Formation outcrop belt in Utah and Arizona with marked study locations at Willow Springs near Tuba City, Arizona, Olsen Canyon within Warner Valley near St. George, Utah, and Blacks Canyon, Utah (within Zion National Park). Image taken from Suarez et al. (2017).

Chapter 3: Methodology

Sampling

Fieldwork was conducted in March of 2018. Three study sites were chosen: Blacks Canyon in Zion National Park, Utah; Olsen Canyon in Warner Valley, and Willow Springs, Arizona. These three study sites were selected to provide a sampling transect of the paleodrainage fluvial system from northwest to southeast (Fig. 2) and to coincide with previous work conducted by Suarez et al. (2017) (Olsen Canyon and Blacks Canyon) and Marsh (2019) (Blacks Canyon and Willow Springs), which provided measured sections and previously collected samples. Each study site was sampled for detrital zircon (DZ) U-Pb geochronology and thin-section petrographic analysis. During March 2018, nine DZ samples were collected at Olsen Canyon (Fig. 4A), nine DZ samples and seven petrographic samples were collected at Blacks Canyon (Fig. 4B), and five DZ samples and ten petrographic samples were collected at Willow Springs (Fig. 4C). In addition to these samples, five DZ samples were collected previously from both Blacks Canyon in 2015 and Willow Springs in 2014 by Marsh (2019) and five petrographic samples were collected previously from Olsen Canyon in 2017 by Suarez et al. (2019) (Table 1).

Table 1: Sample Information

Willow Springs (NE Arizona)

Sample_ID	Formation	Member	Latitude	Longitude
WS 14/01	Chinle	Owl Rock	36.1684	-111.3890
WS 14/02	Moenave	Dinosaur Canyon	36.1684	-111.3890
WS 14/03	Moenave	Dinosaur Canyon	36.1753	-111.3863
WS 14/04	Moenave	Dinosaur Canyon	36.1750	-111.3848
WS 14/05	Moenave	Dinosaur Canyon	36.1748	-111.3814
WS 18/00	Chinle	Owl Rock	36.1683	-111.3891
WS 18/01	Moenave	Dinosaur Canyon	36.1684	-111.3891
WS 18/02	Moenave	Dinosaur Canyon	36.1684	-111.3891
WS 18/03	Chinle	Owl Rock	36.1683	-111.3891
WS 18/04	Moenave	Dinosaur Canyon	36.1751	-111.3863
WS 18/05	Moenave	Dinosaur Canyon	36.1751	-111.3862
WS 18/06	Moenave	Dinosaur Canyon	36.1752	-111.3861
WS 18/07	Moenave	Dinosaur Canyon	36.1749	-111.3849
WS 18/08	Moenave	Dinosaur Canyon	36.1746	-111.3846
WS 18/09	Moenave	Dinosaur Canyon	36.1748	-111.3805
WS 18/10	Moenave	Dinosaur Canyon	36.1742	-111.3821
WS 18/11	Moenave	Dinosaur Canyon	36.1750	-111.3850

Blacks Canyon (SW Utah)

Sample_ID	Formation	Member	Latitude	Longitude
ZS 15/01	Chinle	–	37.1987	-113.0018
ZS 15/02	Moenave	Dinosaur Canyon	37.1994	-113.0008
ZS 15/03	Moenave	Dinosaur Canyon	37.1995	-113.0007
ZS 15/04	Moenave	Dinosaur Canyon	37.1998	-113.0003
ZS 15/05	Moenave	Whitmore Point	37.2009	-113.0049
ZS 18/01	Moenave	Dinosaur Canyon	37.2016	-113.0014
ZS 18/02	Moenave	Dinosaur Canyon	37.2018	-113.0012
ZS 18/03	Moenave	Dinosaur Canyon	37.2018	-113.0010

Table 1: Sample Information Cont.

Blacks Canyon (SW Utah)				
Sample_ID	**Formation**	**Member**	**Latitude**	**Longitude**
ZS 18/05	Moenave	Whitmore Point	37.2019	-113.0009
ZS 18/06	Chinle	–	37.2018	-113.0037
ZS 18/07	Moenave	Dinosaur Canyon	37.2018	-113.0037
ZS 18/08	Chinle	–	37.0014	-113.0014
ZS 18/09	Kayenta	Springdale SS	37.2021	-113.0008

Olsen Canyon (SW Utah)				
Sample_ID	**Formation**	**Member**	**Latitude**	**Longitude**
OC 18/01	Chinle	–	37.0174	-113.3897
OC 18/02	Moenave	Dinosaur Canyon	37.0174	-113.3897
OC 18/03	Moenave	Dinosaur Canyon	37.0174	-113.3897
OC 18/04	Moenave	Dinosaur Canyon	37.0178	-113.3897
OC 18/05	Moenave	Dinosaur Canyon	37.0181	-113.3890
OC 18/06	Moenave	Dinosaur Canyon	37.0182	-113.3889
OC 18/07	Moenave	Dinosaur Canyon	37.0179	-113.3889
OC 18/08	Moenave	Whitmore Point	37.0186	-113.3887
OC 18/09	Kayenta	Springdale SS	37.0194	-113.3893
SS-1	Moenave	Dinosaur Canyon	37.0177	-113.3890
SS-10	Moenave	Dinosaur Canyon	–	–
SS-13	Moenave	Whitmore Point	–	–
SS-15	Moenave	Whitmore Point	37.0186	-113.3887
SS-16	Kayenta	Springdale SS	37.0194	-113.3893

Mineral Separation Methods

Samples were collected to span the uppermost Chinle Formation, the Moenave Formation, and the overlying Springdale Sandstone Member of the Kayenta Formation. Photos were taken of key features, stratigraphic sections, and sampling locations. Samples were then transported back to the University of Arkansas. Following a revised methodology of Dickinson and Gehrels (2008), detrital zircon sandstone samples were processed using standard heavy mineral separation techniques that included (1) disaggregating the sample by crushing and grinding into sand-sized sediment using a jaw crusher and disc mill, (2) hydraulic sorting using a Gemini water table, (3) density separation using lithium heteropolytungstates (LST) heavy liquids (2.85 g/mL), (4) magnetic separation using a Frantz magnetic separator, and (5) density separation using methylene iodide (MEI) heavy liquids (3.28 g/mL). Concentrated aliquots of zircon were mounted on double-stick tape on 1" acrylic round discs and grains were randomly selected for analysis. A total of twenty-five zircon samples were processed and twenty two samples yielded grains (Table 3).

Detrital Zircon U-Pb Analysis

U-Pb analyses were completed at the Trace Element and Radiogenic Isotope Lab (TRAIL) at the University of Arkansas using a Thermo-Scientific iCapQ quadrupole inductively coupled plasma mass spectrometer (ICP-MS) coupled with an Elemental Scientific Inc. NWR 193 Excimer laser ablation system. Each zircon was ablated for 20 seconds using a 25μm spot size with a repetition rate of 10Hz, a helium flow rate of 0.8 L/min, and a fluence of ~4.3 J/cm^2. For each analysis the following isotopes were measured (dwell time in ms): ^{201}Hg (10), ^{202}Hg (10), ^{204}Pb (30), ^{20}6Pb (10), ^{207}Pb (20), ^{208}Pb (10), ^{232}Th (10), and ^{238}U (10). The instrument was tuned so that UO and ThO were <1.0%. Zircon 91500 (1065 Ma; Wiedenbeck et al., 1995) was used as the primary standard, with Plesovice (337.13 Ma; Slama et al., 2008) and R33 (419 Ma; Black et al.,

2004) used as secondary standards (Table 2). Plesovice was used as the primary standard and Zircon 91500 and R33 were used as the secondary standards for the first analysis runs for samples WS 14/01, WS 14/02, WS 14/03, ZS 15/02, ZS 15/03, ZS 15/04. Data reduction was completed using the Iolite v.3.71 (Paton et al., 2011) data reduction and program along with the VisualAge module (Petrus et al., 2012).

The independent variable for detrital zircon analysis is the age measurement from the zircon crystal. The variation in age is determined by the measured isotope ratios between $^{206}Pb/^{238}U$, $^{207}Pb/^{235}U$, and $^{207}Pb/^{206}Pb$. When displaying these ratios, they are plotted on a concordia diagram to assess the degree of concordance for each analysis. When interpreting ages, the $^{206}Pb/^{238}U$ age is typically most precise for <1.2 Ga analyses, while the $^{207}Pb/^{206}Pb$ age is typically most precise for >1.2 Ga analyses (Gehrels 2014). Ratios are considered concordant when the three isotopic ages agree; in this case, the interpreted age is straightforward. Complications arise when an analysis is discordant. Discordance can be attributed to a disturbance in the U-Pb system due to the mobility of Pb after a zircon crystallizes that causes the three critical ratios ($^{206}Pb/^{238}U$, $^{207}Pb/^{235}U$, and $^{206}Pb/^{207}Pb$) to plot off concordia, resulting in a discordant analysis (Gehrels, 2014). A zircon can either inherit Pb or lose Pb, and this decreases the accuracy of age interpretation (Gehrels 2014). Alternatively, discordance can be caused by mixing two age domains (e.g., rim and core), but the likelihood of this occurring is reduced due to the depth profiling method used within this study. For this study an 850 Ma age cutoff was used for determining best age.

Analyses were discarded if one of the following filter criteria were met: $^{207}Pb/^{206}Pb$ age discordance > 30%, $^{207}Pb/^{206}Pb$ age discordance < -15%, $^{206}Pb/^{238}U$ age % 2-sigma error > 10%, $^{206}Pb/^{238}U$ age discordance > 15%. The discordance reported is the $^{206}Pb/^{238}U$ age vs $^{207}Pb/^{206}Pb$ if

older than 850 Ma and $^{206}Pb/^{238}U$ age vs $^{207}Pb/^{235}U$ age if younger than 850 Ma. Furthermore, analyses were discarded if the calculated age was greater than 4.0 Ga.

After the data was reduced and age calculations were determined, detrital zircon U-Pb age distributions were generated as cumulative and relative kernel density estimation plots in Python using detritalPy (Sharman et al., 2018). Provenance analysis was conducted by comparing age distributions from the sampled sandstones with the age ranges of possible source regions (Gehrels, 2014) and published samples from surrounding units (Dickinson and Gehrels, 2008; 2009a; Suarez et al., 2017; Marsh et al., 2019). This study reports a total of 5,190 detrital zircon analyses, including 72 rim and core domains, from 22 samples.

Maximum depositional age calculations follow the procedures outlined by Barbeau et al. (2009), Dickinson and Gehrels (2009b), Zhang et al. (2015), Ross et al. (2016), and Coutts et al. (2019). A total of nine MDA calculations are utilized within this study: youngest single grain (YSG); youngest cluster at 1σ (YC1σ), weighted average of the youngest two or more dates that overlap in error at 1 sigma (Coutts et al., 2019); youngest cluster at 2σ (YC2σ), weighted average of the youngest two or more dates that overlap within uncertainty at 2 sigma (Coutts et al., 2019); youngest detrital zircon (YDZ), performs a Monte Carlo approach to determine a MDA and uncertainty (Coutts et al., 2019); youngest three zircons (Y3Zo), weighted average of the youngest three zircon dates that overlap within uncertainty, and (Y3Za), the weighted average of the youngest three zircon dates present in the sample (Coutts et al., 2019), youngest graphical peak (YPP), the age of the youngest mode in the probability density plot (PDP) of the measured sample population composed of two or more grains (Coutts et al., 2019); youngest statistical population (YSP), weighted average of the youngest sub-sample of two or more grains that yield a MSWD of ~1 (Coutts et al., 2019); tau (τ) method, weighted average of all dates that fall between the

probability minima of the youngest peak (Coutts et al., 2019). Before MDAs were calculated, filters for uranium (U<1000) and discordance (between -5% and <5%) were used to remove potentially problematic young grains between 150-250 Ma. MDA calculations were visualized in stratigraphic height vs. age plots using Python.

Table 2: Secondary Standards Data

Analysis Sequence	*(n=)*	R33 Age (Ma)	% off true age	R33 err2σ	R33 MSWD
J180304_03	12	442.6	5.6%	3.5	1.3
J180304_04_1	7	428.7	2.3%	5.9	1.2
J180304_04_2	9	417	-0.5%	3.3	1.2
J180304_06	19	420.1	0.3%	3.5	4.4
J180304_07	15	420	0.2%	4.8	4.2
J180304_08	13	418.9	0.0%	3.8	1.1
J180304_09	11	420.4	0.3%	2.1	0.5
J180304_10	23	422.6	0.9%	3	3.1
J180304_11a	20	413.5	-1.3%	2.6	1
J180304_11b	14	414.6	-1.1%	5.9	4.2
J180304_12a	20	419.1	0.0%	3.1	1.0
J180304_12b	15	419.1	0.0%	4.8	2.1
J180304_13a	14	419.6	0.1%	6.6	3.4
J180304_13b	13	424	1.2%	4.5	1.8

Analysis Sequence	*(n=)*	Plesovice Age (Ma)	% off true age	Plesovice err2σ	Plesovice MSWD
J180304_06	41	338.3	0.4%	2	8.5
J180304_07	40	332.3	-1.4%	2.4	4.6
J180304_08	37	335.1	-0.6%	1.1	0.42
J180304_09	32	332.9	-1.2%	1.1	0.57
J180304_10	56	347	3.0%	1.4	2.1
J180304_11a	50	344.8	2.3%	1.3	1.0
J180304_11b	38	345	2.4%	2	2.7
J180304_12a	49	336.3	-0.2%	1.5	1.4
J180304_12b	40	347.4	3.1%	1.1	1.4
J180304_13a	38	348	3.3%	1.6	1.3
J180304_13b	40	347.9	3.2%	1.1	0.9

Table 2: Secondary Standards Data Cont.

Analysis Sequence	*(n=)*	91500 Age (Ma)	% off true age	91500 err2σ	91500 MSWD
J180304_03	26	1110.1	4.2%	11	5.1
J180304_04_1	28	1089.7	2.3%	6.7	1.2
J180304_04_2	18	1059.8	-0.5%	4.6	1.2

Petrographic Analysis

Quantitative estimates for sediment composition were made from 26 of 28 thin sections that were prepared by Spectrum Petrographics in Vancouver, Washington. Samples were stained for both plagioclase (red) and potassium feldspar (yellow). Four hundred framework grains were counted per thin section, not including porosity, cement, mica, or other unidentified grains. Ternary plots were generated using Triplot (Thompson, 2009). Q-F-L ternary diagrams were created using the classification scheme developed by Folk (1968, 1980). Qm-F-Lt and Qm-P-K ternary diagrams were created for provenance analysis using the classification schemes developed by Dickinson (1985). The petrographic analysis within this study serves as an alternative method and extra source of information for provenance interpretation.

Table 3: Work Completed

Willow Springs				
Sample_ID	**DZ Sample**	**DZ Processed**	**Yielded Grains**	**Thin Section**
WS 14/01	X	X	X	–
WS 14/02	X	X	X	–
WS 14/03	X	X	X	–
WS 14/04	X	X	–	X
WS 14/05	X	X	–	X
WS 18/00	–	–	–	–
WS 18/01	–	–	–	X
WS 18/02	–	–	–	X
WS 18/03	X	–	–	X
WS 18/04	–	–	–	X
WS 18/05	X	X	X	X
WS 18/06	–	–	–	X
WS 18/07	X	–	–	X
WS 18/08	X	X	X	X
WS 18/09	X	X	X	X
WS 18/10	–	–	–	–
WS 18/11	–	–	–	–

Blacks Canyon				
Sample_ID	**DZ Sample**	**DZ Processed**	**Yielded Grains**	**Thin Section**
ZS 15/01	X	–	–	–
ZS 15/02	X	X	X	–
ZS 15/03	X	X	X	–
ZS 15/04	X	X	X	–
ZS 15/05	X	X	–	–
ZS 18/01	X	X	X	X
ZS 18/02	X	X	X	X
ZS 18/03	X	X	X	X

Table 3: Work Completed Cont.

Blacks Canyon				
Sample_ID	**DZ Sample**	**DZ Processed**	**Yielded Grains**	**Thin Section**
ZS 18/05	X	X	X	X
ZS 18/06	X	–	–	–
ZS 18/07	X	X	X	X
ZS 18/08	X	–	–	–
ZS 18/09	–	–	–	X
Olsen Canyon				
Sample_ID	**DZ Sample**	**DZ Processed**	**Yielded Grains**	**Thin Section**
OC 18/01	X	–	–	–
OC 18/02	X	X	X	–
OC 18/03	X	X	X	–
OC 18/04	X	X	X	X
OC 18/05	X	X	X	X
OC 18/06	X	X	X	X
OC 18/07	X	X	X	–
OC 18/08	X	X	X	X
OC 18/09	X	–	–	X
SS-1	–	–	–	X
SS-10	–	–	–	X
SS-13	–	–	–	X
SS-15	–	–	–	X
SS-16	–	–	–	X

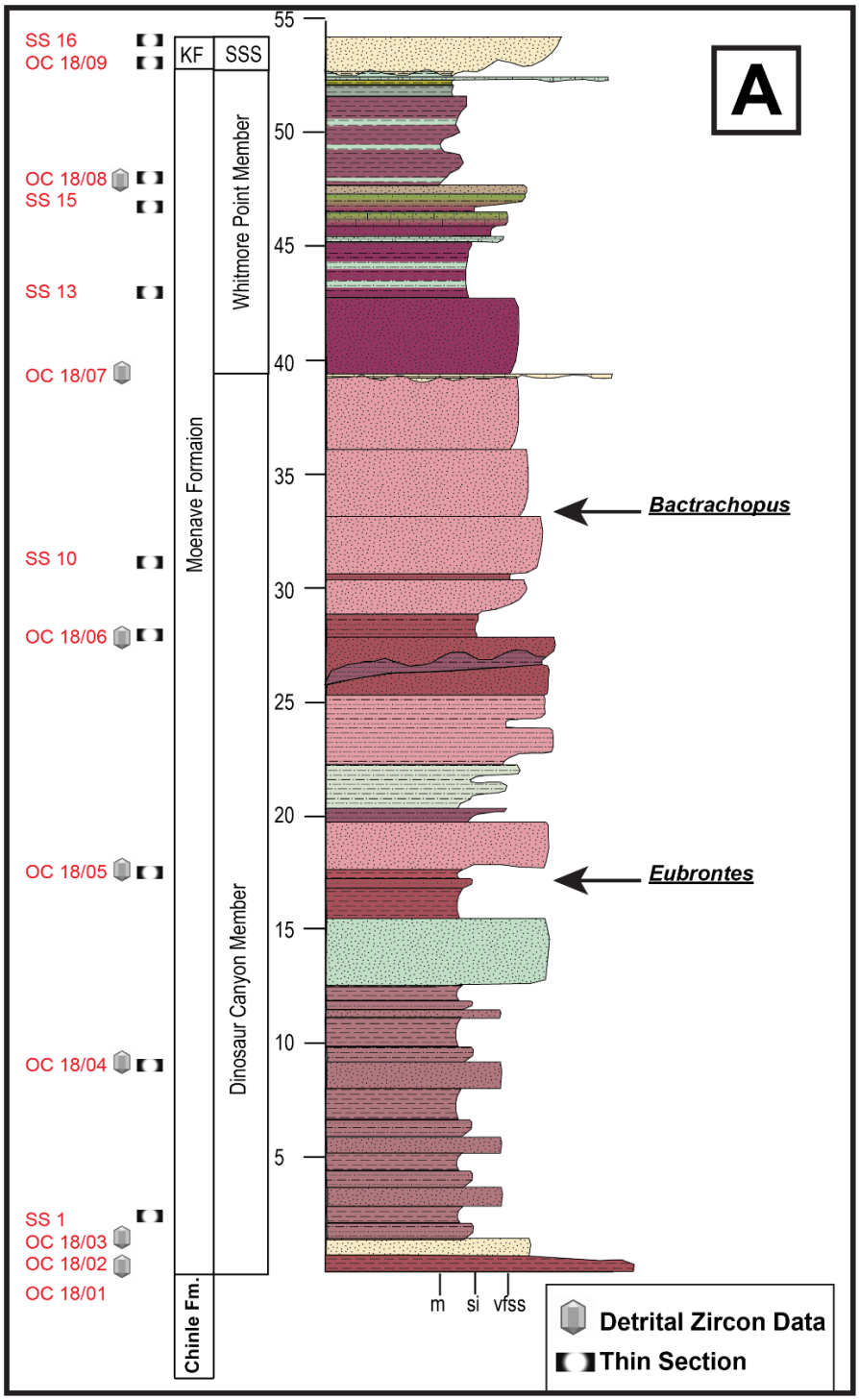

Figure 4: A.) Measured stratigraphic section at Olsen Canyon modified from Suarez et al. (2017) and Oefinger (unpublished) with collected detrital zircon and petrographic sample locations posted and locations of biostratigraphic indicators. **B.)** Measured stratigraphic section at Blacks Canyon modified from Suarez et al. (2017) with collected detrital zircon and petrographic sample locations posted. **C.)** Measured stratigraphic section of Willow Springs from Marsh (2019) with collected detrital zircon and petrographic sample locations posted.

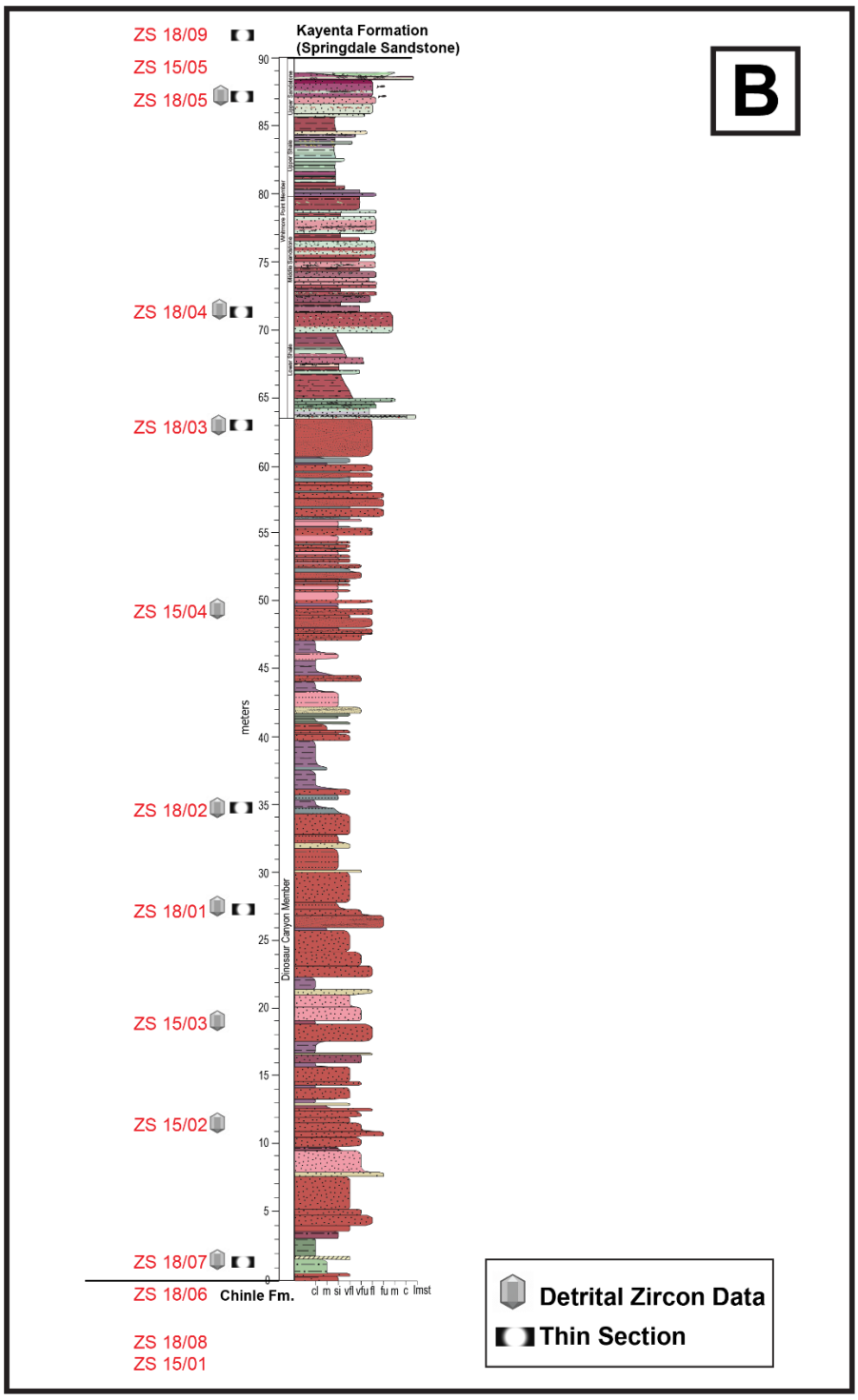

Figure 4 Cont.

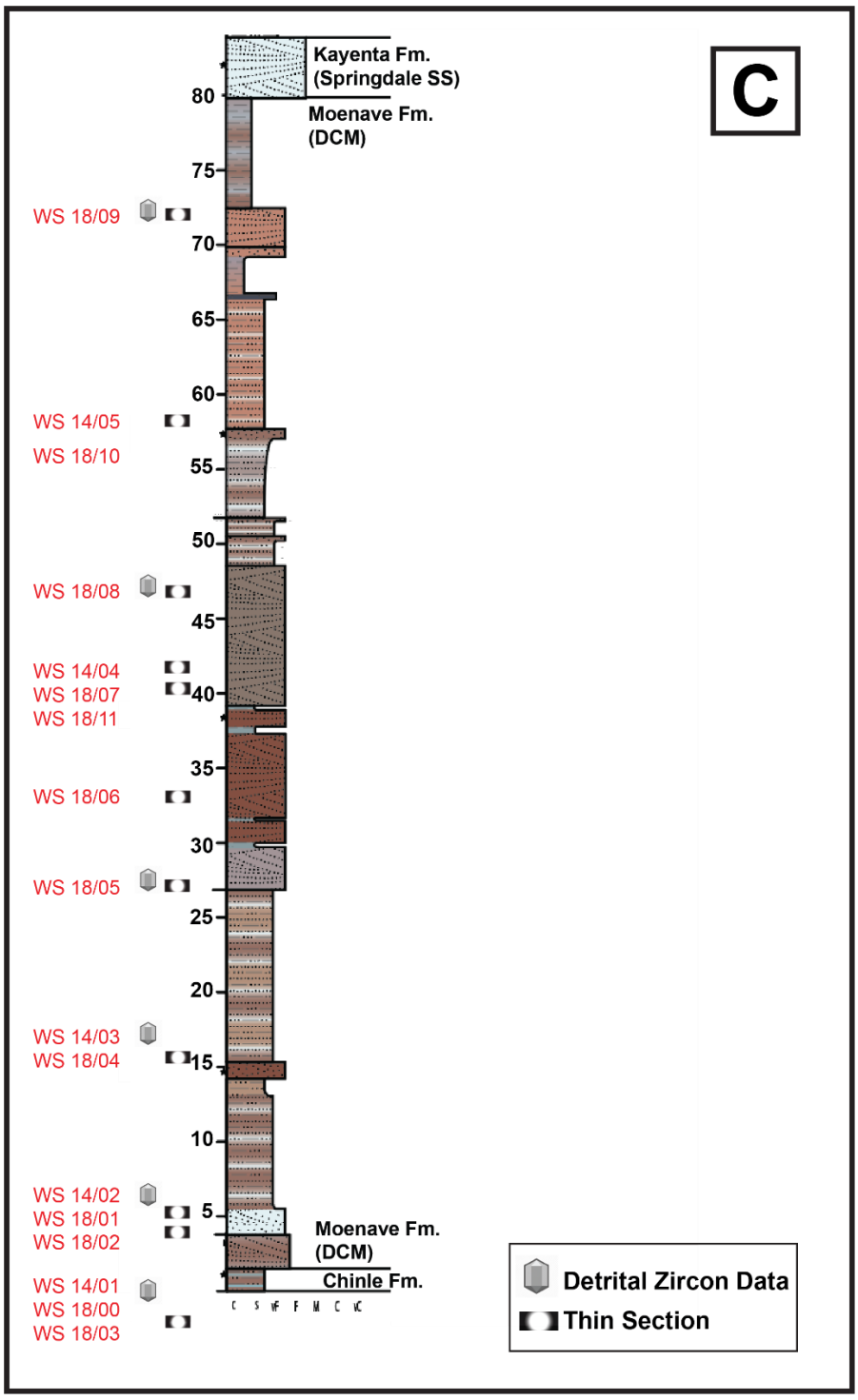

Figure 4 Cont.

Chapter 4: Results

U-Pb Age Distributions

All detrital zircon U-Pb data are found in Appendix A, and data for standards are found in Appendix B. This study reports detrital zircon U-Pb age distributions, age peaks, and age abundances present within the Moenave Formation (Table 4), using observations made from individual samples (Fig. 6) and from a compilation of all Moenave Formation samples (*n*=5159, 21 samples, Fig. 5).

Table 4: Summary of Moenave Formation Age Populations (0-3000 Ma) of 5159 Detrital Zircon Analyses

Interpreted Sediment Source	Age Peak(s) (Ma)	Binned Age Range (Ma)	Number of Grains	Percentage of Grains
Cordilleran arc	206	<300	337	6.53%
Appalachian and peri-Gondwanan	402 & 571	300-800	2195	42.55%
Grenville	1045	800-1300	1191	23.09%
Mesoproterozoic plutonic	1422	1300-1550	441	8.55%
Yavapai-Mazatzal	1684	1550-1800	562	10.89%
N. Laurentia	1912	>1800	433	8.39%

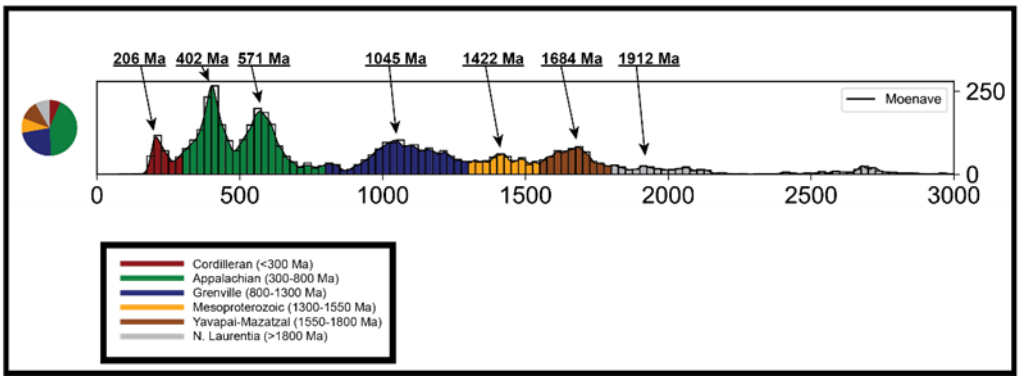

Figure 5: Compiled detrital zircon U-Pb age distribution (0-3000 Ma) of all Moenave Formation samples collected (*n*=5145/5159). Distribution is a KDE with a bandwidth of 10 Myr. Pie charts are reported to visualize percent abundance of age populations. Age peak values are reported above the plot with arrows indicating the corresponding peak. Coloring corresponds with the map of North American basement provinces and their crystallization age (Table 4, Fig. 1).

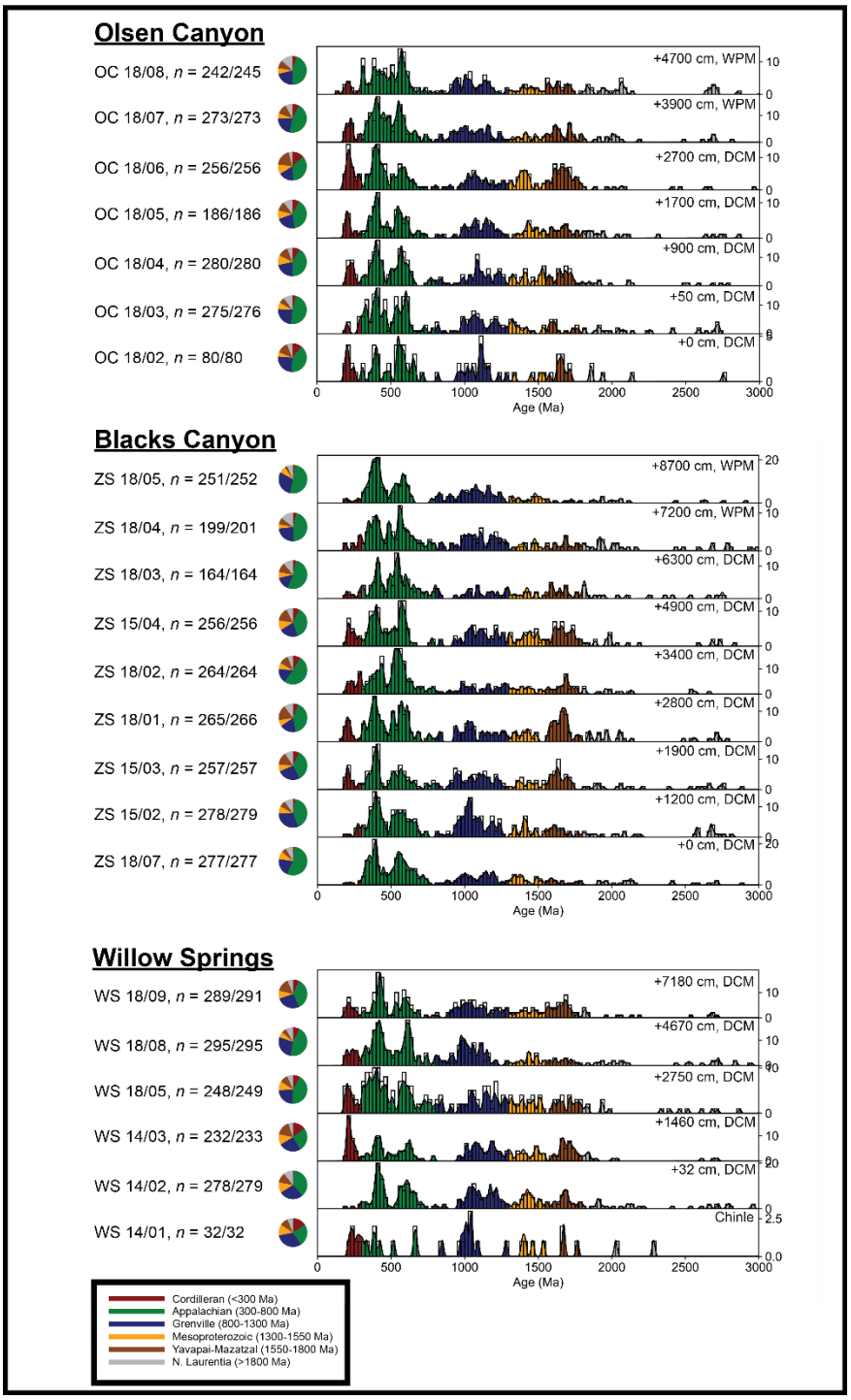

Figure 6: Detrital zircon U-Pb age distributions (0-3000 Ma). Data are displayed by study site and in stratigraphic order. Distributions are KDEs with a bandwidth of 10 Myr. Pie charts are reported to visualize percent abundance of age populations. Coloring corresponds with the map of North American basement provinces and their crystallization age (Table 4, Fig. 1). Sample names and number of analyses plotted/total number of analyses within each plot are reported to the left. Lithologic members and stratigraphic height above the Chinle are reported to the right.

Moenave Formation samples contain grain age populations of Mesozoic Cordilleran arc ages (50-300 Ma), Appalachian and peri-Gondwanan ages (300-800 Ma), Grenvillian ages (800-1300 Ma), Mesoproterozoic pluton ages (1300-1550 Ma) Yavapai-Mazatzal ages (1550-1800 Ma), and North Laurentia ages (greater than 1800 Ma). The combined detrital age spectrum for the Moenave Formation is characterized by a dominant Appalachian and peri-Gondwanan age population (42.55%) with two distinctive age peaks, a Paleozoic age peak (402 Ma) and a Neoproterozoic age peak (571 Ma). This is followed by a broad Grenvillian age population (23.09%). The next largest detrital age components are of Yavapai-Mazatzal age (10.89%), Mesoproterozoic plutons age (8.55%), North Laurentia age (8.39%), and Mesozoic Cordilleran arc age (6.53%) which has one distinctive age peak (206 Ma).

Inspection of individual sample age distribution plots (Fig. 6) shows that age populations of detrital zircons in all Moenave samples are broadly similar. The major difference is in the variable content of grains younger than 300 Ma derived from the Cordilleran magmatic arc. Table 5 provides a comparison of the arc peak abundance of individual samples. The samples that yielded the largest supply of arc derived grains occur in the lower-middle DCM (Willow Springs: 7.22%, 7.46%, 8.03%, 14.59%; Blacks Canyon: 6.02%, 7.0%, 7.42%, 8.71%; Olsen Canyon: 8.06%, 8.57%, 13.67%), while the samples that yielded the smallest amount of arc derived grains seem to occur at the basal DCM (Willow Springs: 1.43%; Blacks Canyon: 1.81%; Olsen Canyon: 3.99%), with the exception of OC 18/02 (11.25%), and within the WPM (Blacks Canyon: 2.38%, 3.98%; Olsen Canyon: 4.9%). It should also be noted that samples with higher abundances of arc-derived zircon also had higher abundances of Yavapai-Mazatzal ages.

Table 5: Potential Arc Peak Abundance Controls Within Individual Samples

Sample	Member	*(n=)*	Arc Peak Abundance	Stratigraphic Height (m)	Depositional Environment	Grain Size
Willow Springs						
WS 18/09	DCM	21	7.22%	71.8	Fluvial	fs
WS 18/08	DCM	22	7.46%	46.7	Eolian	fs
WS 18/05	DCM	20	8.03%	27.5	Fluvial	vfs
WS 14/03	DCM	34	14.59%	14.6	Fluvial	vfs
WS 14/02	DCM	4	1.43%	3.2	Fluvial	vfs
WS 14/01	Owl Rock	5	15.63%	1	Fluvial	vf siltstone
Blacks Canyon						
ZS 18/05	WPM	6	2.38%	87	Lacustrine	vfs
ZS 18/04	WPM	8	3.98%	72	Lacustrine	vfs
ZS 18/03	DCM	6	3.66%	63	Fluvial	vfs
ZS 15/04	DCM	19	7.42%	49	Fluvial	vfs
ZS 18/02	DCM	23	8.71%	34	Fluvial	vfs
ZS 18/01	DCM	16	6.02%	28	Fluvial	coarse silt
ZS 15/03	DCM	18	7.00%	19	Fluvial	vfs
ZS 15/02	DCM	8	2.87%	12	Fluvial	vfs
ZS 18/07	DCM	5	1.81%	0	Fluvial	vfs
Olsen Canyon						
OC 18/08	WPM	12	4.9%	47	Lacustrine	coarse silt
OC 18/07	WPM	21	7.69%	39	Lacustrine	vfs
OC 18/06	DCM	35	13.67%	27	Fluvial	coarse silt
OC 18/05	DCM	15	8.06%	17	Fluvial	coarse silt
OC 18/04	DCM	24	8.57%	9	Fluvial	vfs
OC 18/03	DCM	11	3.99%	0.5	Fluvial	vfs
OC 18/02	DCM	9	11.25%	0	Fluvial	vfs

Maximum Depositional Age

This study reports a total of nine MDA calculations filtered for uranium (U<1000) and discordance (between -5% and 5%), based on methods outlined in Barbeau et al. (2009), Dickinson and Gehrels (2009b), Zhang et al. (2016), Ross et al. (2017), and Coutts et al. (2019). Table 6 reports the filtered results of the MDA calculations for individual samples, grouped by study site and listed in stratigraphic order, with number of grains included (*n=)*, 2σ absolute error, % discordance for YSG, and mean-square weighted deviations (MSWD) for the mean ages. Figure 7 visualizes individual sample MDA calculations in stratigraphic height versus age plots.

Table 6: Filtered Detrital Zircon U-Pb MDA Calculations for Individual Moenave Samples

Sample	Filtered Grains	YSG	YSG err2σ	YSG %Disc	YC1σ	YC1σ err2σ	YC1σ MSWD	YC1σ *(n=)*
WS 18/09	193	177.4	4.2	2	207.7	4.2	0.6	3
WS 18/08	215	191.5	6.3	1.5	191.4	4.5	0.0	2
WS 18/05	120	194	6.8	0	195.7	3.6	0.1	3
WS 14/03	142	197.8	5.3	-1.3	199.8	2.9	0.4	3
WS 14/02	183	192.5	7.1	2.3	389.5	4.4	0.1	5
WS 14/01	15	213.4	5.3	3.4	1005.2	33.3	0.8	2
ZS 18/05	133	197	4.5	1.0	339.9	4.1	0.13	4
ZS 18/04	93	188	11	0.5	193.6	6.3	1.6	2
ZS 18/03	57	201	7.4	2.9	287.1	4.9	2.0	2
ZS 15/04	145	196.2	6.6	-1.1	202.6	2.8	0.4	2
ZS 18/02	101	197.5	7	3.2	200.0	3.6	0.4	3
ZS 18/01	150	169.6	5.2	-2.5	190.0	3.9	1.4	2
ZS 15/03	166	198.6	7.8	-3.4	202.4	2.3	0.6	6
ZS 15/02	178	273.5	4.8	1.4	349.1	5.0	1.6	2
ZS 18/07	134	190.6	4.5	-0.3	345.2	2.9	0.3	4
OC 18/08	129	139.7	3.7	4.0	199.9	2.8	0.8	2
OC 18/07	154	189.8	5.6	2.2	221.9	2.9	0.1	2
OC 18/06	127	193.1	6.1	3.9	195.0	3.5	0.5	2
OC 18/05	101	200.9	3.5	3.69	200.8	2.5	0.0	2
OC 18/04	136	202.2	4.1	-0.1	219.9	3.3	0.3	2
OC 18/03	155	201.1	5.6	-1.6	292.4	4.5	1.2	2
OC 18/02	38	203.8	5.7	4.3	252.7	4.7	1.5	2

Sample	YC2σ	YC2σ err2σ	YC2σ MSWD	YC2σ *(n=)*	YDZ mode	YDZ err2σ+	YDZ err2σ-
WS 18/09	209.8	7.1	0.3	4	177.30	4.1	3.9
WS 18/08	195.3	6.6	0.5	4	188.94	5.6	4.8
WS 18/05	195.7	7.3	0.0	3	193.74	3.6	8.1
WS 14/03	202.9	4.1	0.4	6	197.42	3.5	4.8
WS 14/02	397.5	5.3	0.4	12	193.57	5.8	8.0
WS 14/01	1022.8	50.1	0.2	4	212.79	5.7	4.6
ZS 18/05	339.9	8.3	0.0	3	197.55	3.9	5.0
ZS 18/04	341.1	7.7	0.5	4	189.67	7.2	12.3
ZS 18/03	288.6	9.3	0.7	3	201.37	6.8	7.8
ZS 15/04	201.6	5.1	0.4	3	196.44	5.0	6.8
ZS 18/02	201.8	5.5	0.3	5	196.34	4.8	5.9
ZS 18/01	193.4	5.7	0.6	4	170.06	4.5	5.6
ZS 15/03	203.7	4.2	0.3	7	196.60	4.0	9.4
ZS 15/02	355.4	5.9	0.4	9	273.18	4.8	4.6

Table 6: Filtered Detrital Zircon U-Pb MDA Calculations for Individual Moenave Samples Cont.

Sample	YC2σ	YC2σ err2σ	YC2σ MSWD	YC2σ *(n=)*	YDZ mode	YDZ err2σ+	YDZ err2σ-
ZS 18/07	348.0	4.8	0.8	5	190.63	4.4	4.4
OC 18/08	312.5	6.4	0.3	5	139.63	3.5	3.5
OC 18/07	223.0	5.3	0.3	3	190.21	4.7	5.8
OC 18/06	197.0	5.8	0.4	4	193.14	3.9	6.2
OC 18/05	214.9	5.2	0.1	4	199.70	2.9	3.1
OC 18/04	234.7	4.4	0.3	4	201.87	4.3	3.7
OC 18/03	294.4	6.3	0.2	4	201.43	5.1	5.8
OC 18/02	547.7	8.8	0.1	4	204.17	4.9	5.9

Sample	Y3Za	Y3Za err2σ	Y3Za MSWD	Y3Zo	Y3Zo err2σ	Y3Zo MSWD	YPP
WS 18/09	186.0	3.2	26.3	207.7	4.2	0.6	207.7
WS 18/08	194.1	3.6	2.0	194.1	3.6	2.0	191.9
WS 18/05	195.7	3.6	0.1	195.7	3.6	0.1	195.9
WS 14/03	199.8	2.9	0.4	199.8	2.9	0.4	206.6
WS 14/02	253.0	3.3	394.5	390.0	4.7	0.0	391.3
WS 14/01	274.7	2.6	384.2	1015.9	28.1	1.1	1021.9
ZS 18/05	224.1	2.7	156.0	339.9	4.1	0.1	313.8
ZS 18/04	224.6	3.8	73.0	340.3	3.9	1.9	195.4
ZS 18/03	238.0	4.0	146.0	288.6	4.6	3.0	286.0
ZS 15/04	201.6	2.5	1.8	201.6	2.5	1.8	202.4
ZS 18/02	200.0	3.6	0.4	200.0	3.6	0.4	202.1
ZS 18/01	182.5	3.1	20.2	192.7	3.0	3.0	191.5
ZS 15/03	199.0	4.6	0.0	202.0	3.0	0.8	203.1
ZS 15/02	289.3	3.1	40.8	351.1	4.2	1.8	273.6
ZS 18/07	224.8	3.0	316.5	344.5	3.3	0.1	345.5
OC 18/08	165.8	2.4	205.3	312.0	3.5	2.0	200.3
OC 18/07	197.0	3.2	6.2	223.0	2.6	1.5	190.4
OC 18/06	196.6	3.0	2.0	196.6	3.0	2.0	195.9
OC 18/05	203.0	2.3	8.8	214.6	2.6	0.0	200.8
OC 18/04	209.5	2.4	12.8	234.3	2.3	1.7	220.2
OC 18/03	220.4	3.6	115.9	293.6	3.6	1.0	294.9
OC 18/02	211.6	3.5	20.1	546.7	4.7	0.1	253.8

Sample	YSP	YSP err2σ	YSP MSWD	tauMethod	tauMethod err2σ	tauMethod MSWD	tauMethod *(n=)*
WS 18/09	207.7	4.2	0.6	207.7	4.2	0.6	3
WS 18/08	191.4	4.5	0.0	206.9	2.8	0.1	2
WS 18/05	195.5	3.9	0.3	195.7	3.6	0.2	3

Table 6: Filtered Detrital Zircon U-Pb MDA Calculations for Individual Moenave Samples Cont.

Sample	YSP	YSP err2σ	YSP MSWD	tauMethod	tauMethod err2σ	tauMethod MSWD	tauMethod *(n=)*
WS 14/03	200.9	2.5	0.9	204.1	1.8	2.5	7
WS 14/02	391.6	3.9	0.9	387.9	4.2	1.6	6
WS 14/01	1022.8	25.1	1.1	1022.8	25.1	1.1	4
ZS 18/05	339.9	4.1	0.1	339.9	4.1	0.1	4
ZS 18/04	243.1	3.7	0.2	341.1	3.9	2.3	4
ZS 18/03	404.2	4.5	1.1	400.6	3.8	3.6	4
ZS 15/04	202.6	2.8	0.4	201.6	2.6	1.8	3
ZS 18/02	201.8	2.7	1.2	201.8	2.8	1.2	5
ZS 18/01	197.5	4.3	0.1	190.1	3.9	1.4	2
ZS 15/03	202.4	2.3	0.6	203.7	2.1	1.5	7
ZS 15/02	356.8	3.1	0.9	356.0	2.9	1.8	10
ZS 18/07	345.8	2.8	0.8	345.2	2.9	0.3	4
OC 18/08	199.9	2.8	0.8	314.1	2.9	1.8	7
OC 18/07	223.0	2.6	1.5	221.9	3.0	0.2	2
OC 18/06	195.0	3.5	0.5	197.0	2.9	1.7	4
OC 18/05	200.8	2.5	0.1	214.9	2.6	0.4	4
OC 18/04	219.9	3.3	0.3	233.9	2.1	2.3	5
OC 18/03	295.3	3.3	0.3	294.4	3.2	0.9	4
OC 18/02	547.7	4.4	0.4	547.7	4.4	0.4	4

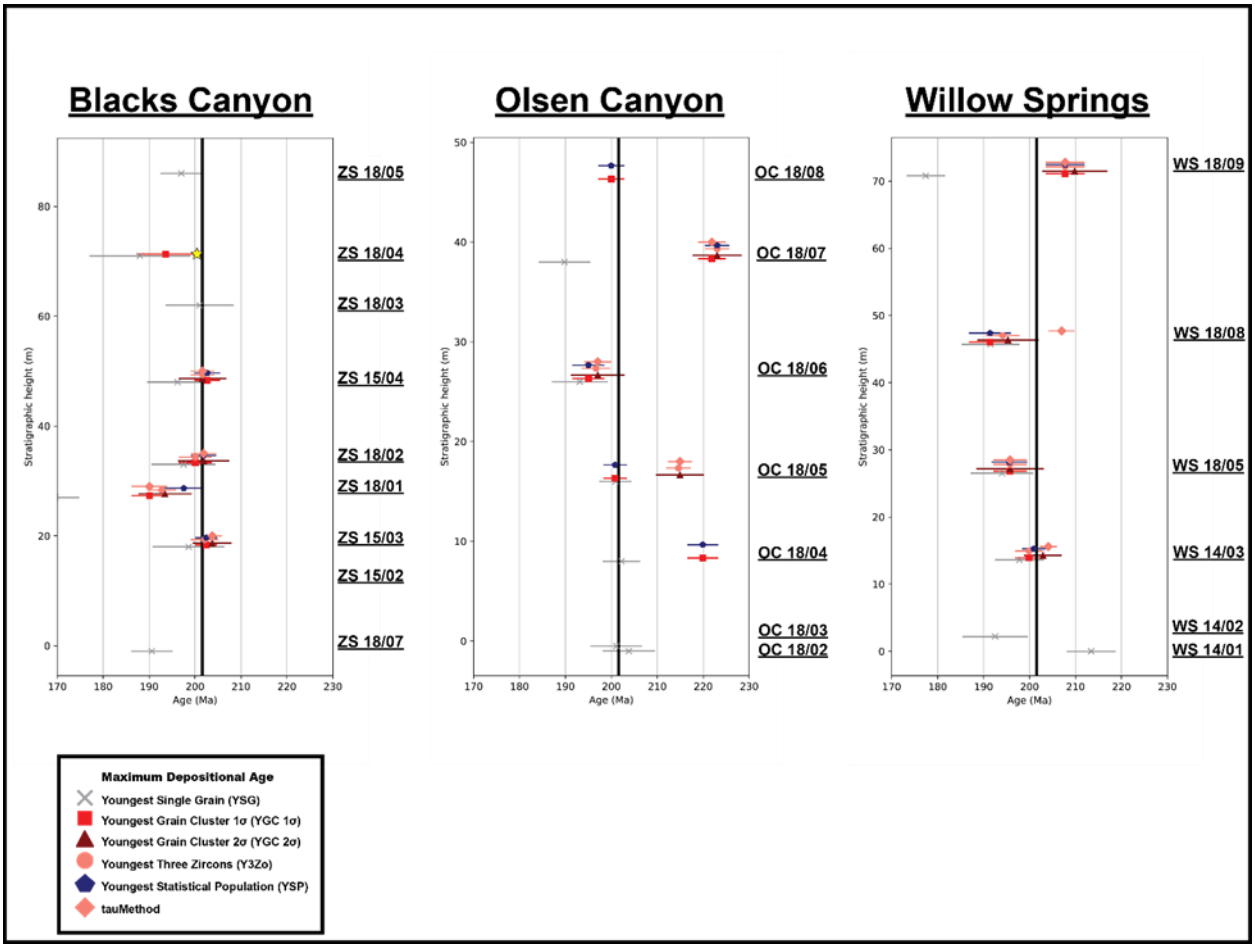

Figure 7: MDA calculations of individual samples, separated into study site locations, plotted stratigraphic height (meters) vs. age (170-230 Ma). The middle black line represents the age of the ETE (201.564 ± 0.015 M.) (Blackburn et al., 2013). The yellow star placed at the same stratigraphic height as sample ZS 18/04 in the Blacks Canyon section represents the location and age of the TIMS sample ZWP-2015 (201.28 ± 0.11/0.15 Ma) reported by Suarez et al. (2017).

Sandstone Petrofacies

Four hundred framework grains were counted for each of 26 thin sections, not including porosity, cement, mica, or other unidentified grains (Table 7, Fig. 8). Table 8 provides recalculated modal percentages of detrital modes to determine values of total quartzose grains (Q), total monocrystalline quartz (Qm), total feldspar grains (F), total plagioclase grains (P), total potassium feldspar grains (K), total lithics (L), and total lithics including polycrystalline quartz (Lt), which are needed to plot Q-F-L and Qm-F-Lt ternary plots. The majority of samples are very fine-grained sandstones with some instances of coarse-grained siltstones (3 samples) and fine-grained sandstones (5 samples) (Table 8). Samples consist of sub-angular to sub-rounded grains and are mostly well-sorted with some being poorly sorted (WS 18/01, WS 18/02, WS 18/09). Samples range between arkose and subarkose (Fig. 8A) in the classification of Folk (1968,1980). The same results are obtained when using the classification of McBride (1963) except for some Willow Springs samples that plot in the lithic subarkose range (Fig. 8B). Thin section microphotographs have been provided to give a visual representation for these descriptions (Fig. 9).

Table 7: Detrital Modes from Sandstones of the Moenave Formation

Sample	Qm	Qpc	Qpo	K	P	Lsm	Lvm	Mm	Mb	O	Grain Size
Olsen Canyon											
SS-16	289	8	13	49	53	1	0	1	2	4	fs
OC 18/09	297	2	19	35	46	1	0	1	0	3	fs
OC 18/08	266	2	10	62	60	0	0	2	1	4	vfs
SS-15	278	2	7	47	66	0	0	4	1	1	vfs
SS-13	282	1	6	41	69	0	0	3	0	9	vfs
OC 18/06	248	0	9	64	79	0	0	4	4	10	css
OC 18/05	292	0	11	61	30	5	0	5	11	18	css
OC 18/04	261	3	12	41	81	2	0	1	0	8	vfs
SS-1	286	2	9	39	63	1	0	3	0	4	vfs
Willow Springs											
WS 18/09	283	0	33	65	19	0	0	0	1	3	fs
WS 14/05	264	0	28	76	14	0	13	0	0	5	vfs
WS 18/08	283	1	30	59	14	0	13	0	0	0	fs
WS 14/04	267	1	32	63	35	0	1	3	4	1	vfs
WS 18/07	274	0	43	48	22	2	7	0	0	4	vfs
WS 18/06	277	0	38	57	13	0	15	8	3	10	vfs
WS 18/05	264	0	16	61	58	0	1	1	0	6	vfs
WS 18/04	249	1	25	77	39	1	1	1	0	7	vfs
WS 18/01	255	0	33	54	39	0	17	0	0	2	vfs
WS 18/02	286	0	30	49	31	1	1	0	3	2	vfs
Blacks Canyon											
ZS 18/09	279	0	9	63	48	0	1	1	1	2	fs
ZS 18/05	296	0	14	65	25	0	0	4	0	3	vfs
ZS 18/04	216	0	25	79	61	0	14	5	6	5	vfs
ZS 18/03	256	0	19	55	48	0	16	3	2	7	vfs
ZS 18/02	267	1	14	63	44	0	1	2	2	10	vfs
ZS 18/01	271	0	10	50	36	0	16	0	0	17	css
ZS 18/07	262	0	18	55	54	0	5	3	4	6	vfs

Notes: Modes are based on point counts of 400 framework grains not including porosity, cement, mica, or other unidentified grains. Monocrystalline grains: Qm—monocrystalline quartz; P—plagioclase feldspar; K—potassium feldspar. Polycrystalline grains: Qpc—microcrystalline quartz (dominantly chert); Qpo—polycrystalline quartz (equant, stretched, or vein quartz); Lvm—volcanic and metavolcanic lithic fragments; Lsm—sedimentary and metasedimentary lithic fragments. Mm—mica flakes (muscovite); Mb—mica flakes (biotite). O—Other unidentified grains. Grain Size: fs—fine-grained sand; vfs—very fine-grained sand; css—coarse-grained silt. Samples are grouped by study site and listed in stratigraphic order

Table 8: Recalculated Modal Percentages of Sandstone from the Moenave Formation

	Q-F-L (%)			Qm-F-Lt (%)			Qm-P-K (%)			
Sample	**Qm**	**F**	**L**	**Qm**	**F**	**Lt**	**Qm**	**P**	**K**	**Grain Size**
Olsen Canyon										
SS-16	75	25	0	70	25	5	74	14	13	fs
OC 18/09	80	20	0	74	20	6	79	12	9	fs
OC 18/08	70	31	0	67	31	3	69	15	16	vfs
SS-15	72	28	0	70	28	2	71	17	12	vfs
SS-13	72	28	0	71	28	2	72	18	10	vfs
OC 18/06	64	36	0	62	36	2	63	20	16	css
OC 18/05	76	23	1	73	23	4	76	8	16	css
OC 18/04	69	31	1	65	31	4	68	21	11	vfs
SS-1	74	26	0	72	26	3	74	16	10	vfs
Willow Springs										
WS 18/09	79	21	0	71	21	8	77	5	18	fs
WS 14/05	74	23	3	67	23	10	75	4	21	vfs
WS 18/08	79	18	3	71	18	11	79	4	17	fs
WS 14/04	75	25	0	67	25	9	73	10	17	vfs
WS 18/07	80	18	2	69	18	13	80	6	14	vfs
WS 18/06	79	18	4	69	18	13	80	4	16	vfs
WS 18/05	70	30	0	66	30	4	69	15	16	vfs
WS 18/04	70	30	1	63	30	7	68	11	21	vfs
WS 18/01	72	23	4	64	23	13	73	11	16	vfs
WS 18/02	79	20	1	72	20	8	78	8	13	vfs
Blacks Canyon										
ZS 18/09	72	28	0	70	28	3	72	12	16	fs
ZS 18/05	78	23	0	74	23	4	77	6	17	vfs
ZS 18/04	61	35	4	55	35	10	61	17	22	vfs
ZS 18/03	70	26	4	65	26	9	71	13	15	vfs
ZS 18/02	72	27	0	68	27	4	71	12	17	vfs
ZS 18/01	73	22	4	71	22	7	76	10	14	css
ZS 18/07	71	28	1	66	28	6	71	15	15	vfs

Notes: Q—total quartzose grains (Qm + Qpc + Qpo). F—total feldspar grains (K + P). L—total aphanitic lithic fragments (Lvm + Lsm), Lt—total aphanitic lithic fragments including polycrystalline quartz (L + Qp). Grain Size: fs—fine-grained sand; vfs—very fine-grained sand; css—coarse-grained silt. Samples are grouped by study site and listed in stratigraphic order

Ternary Provenance Description

Figure 10A provides a graphical representation of different tectonic settings using the classification scheme of Dickinson (1985), which serves as a complimentary method and extra source of information for provenance interpretation when paired with detrital zircon U-Pb ages. All sandstone samples of the Moenave Formation plot within the transitional continental provenance type. Two eolian samples (WS 18/07 and WS 18/08) plot approximately on the border of the transitional continental terrane and the quartzose recycled terrane (Fig. 10A). Observing Figure 10B, Dickinson and Suczek (1979) and Dickinson (1985) describe the more feldspathic end of the trend as sands derived mainly from magmatic arcs, and the more quartzose end of the trend as sands derived from continental blocks or recycled through derivative orogenic terranes. All sandstone samples of the Moenave Formation plot toward the quartzose end of this trend (Fig. 10B).

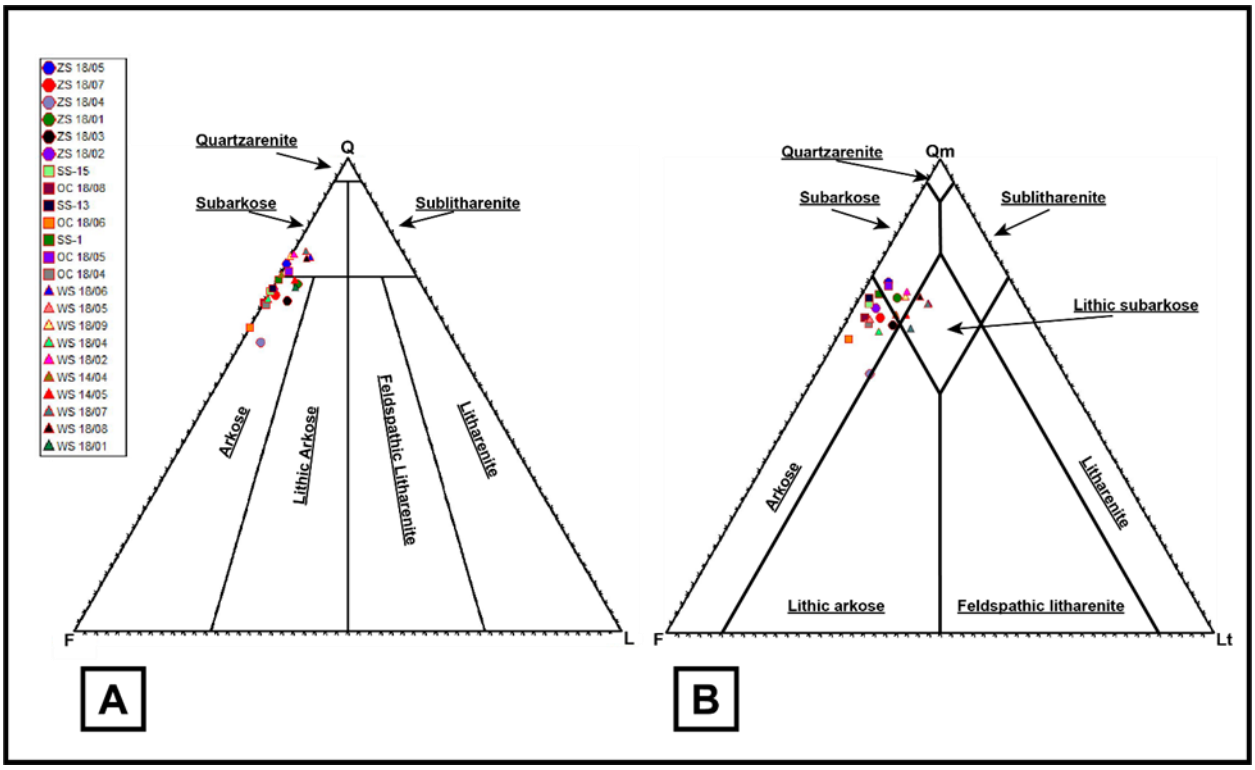

Figure 8: A.) Q-F-L ternary diagram of sandstones from the Moenave Formation using the classification scheme developed by Folk (1968, 1980). **B.)** Qm-F-Lt ternary diagram of sandstones from the Moenave Formation using the classification scheme developed by McBride (1963).

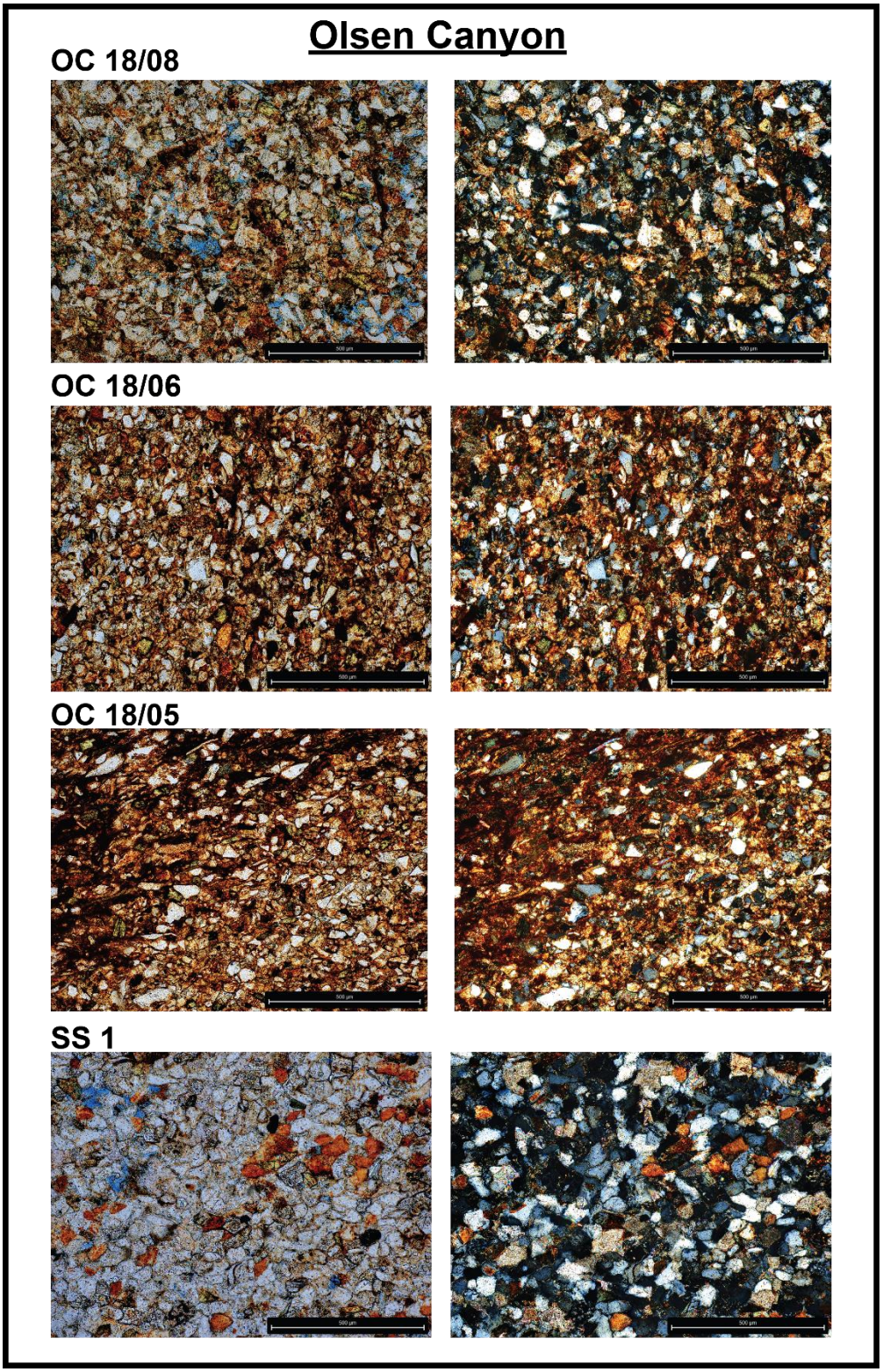

Figure 9: Thin section microphotographs of the Moenave Formation. Sample images were selected to give a stratigraphic overview of each section. Sample microphotographs are presented in pairs, images on the left were taken in plain light and images on the right were taken in cross polarized light. Scale bar on all images represents 500 microns.

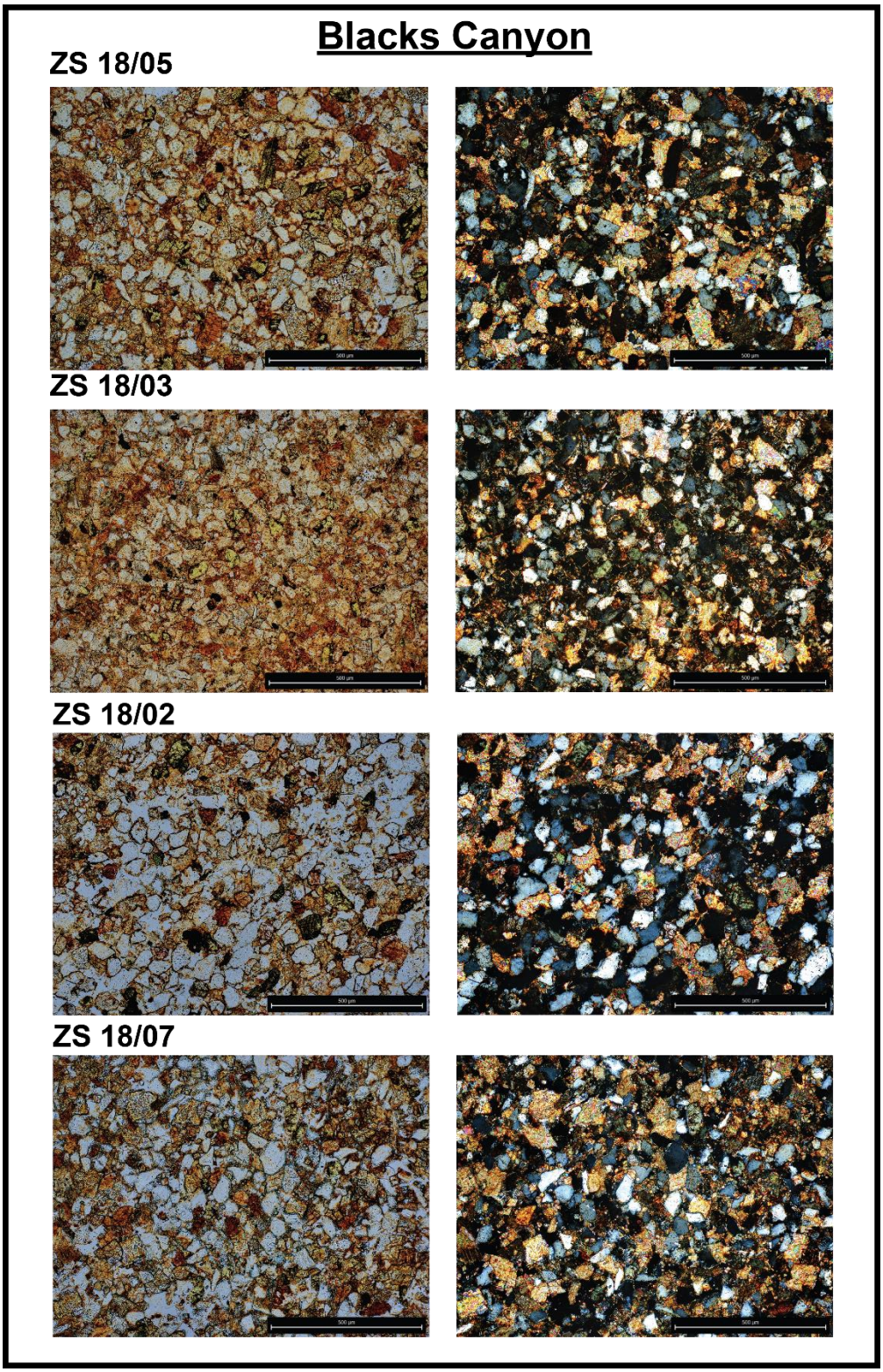

Figure 9 Cont.

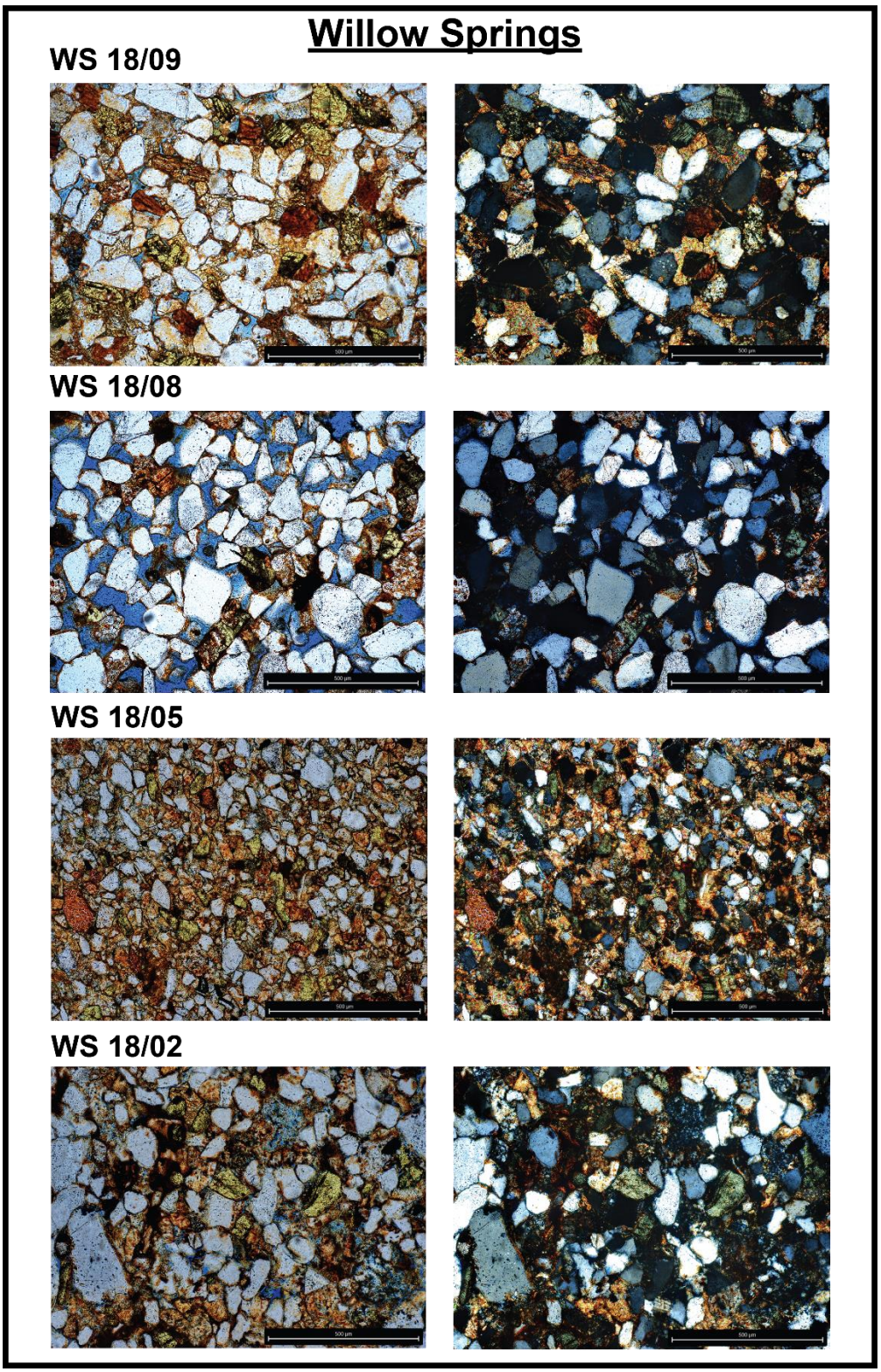

Figure 9 Cont.

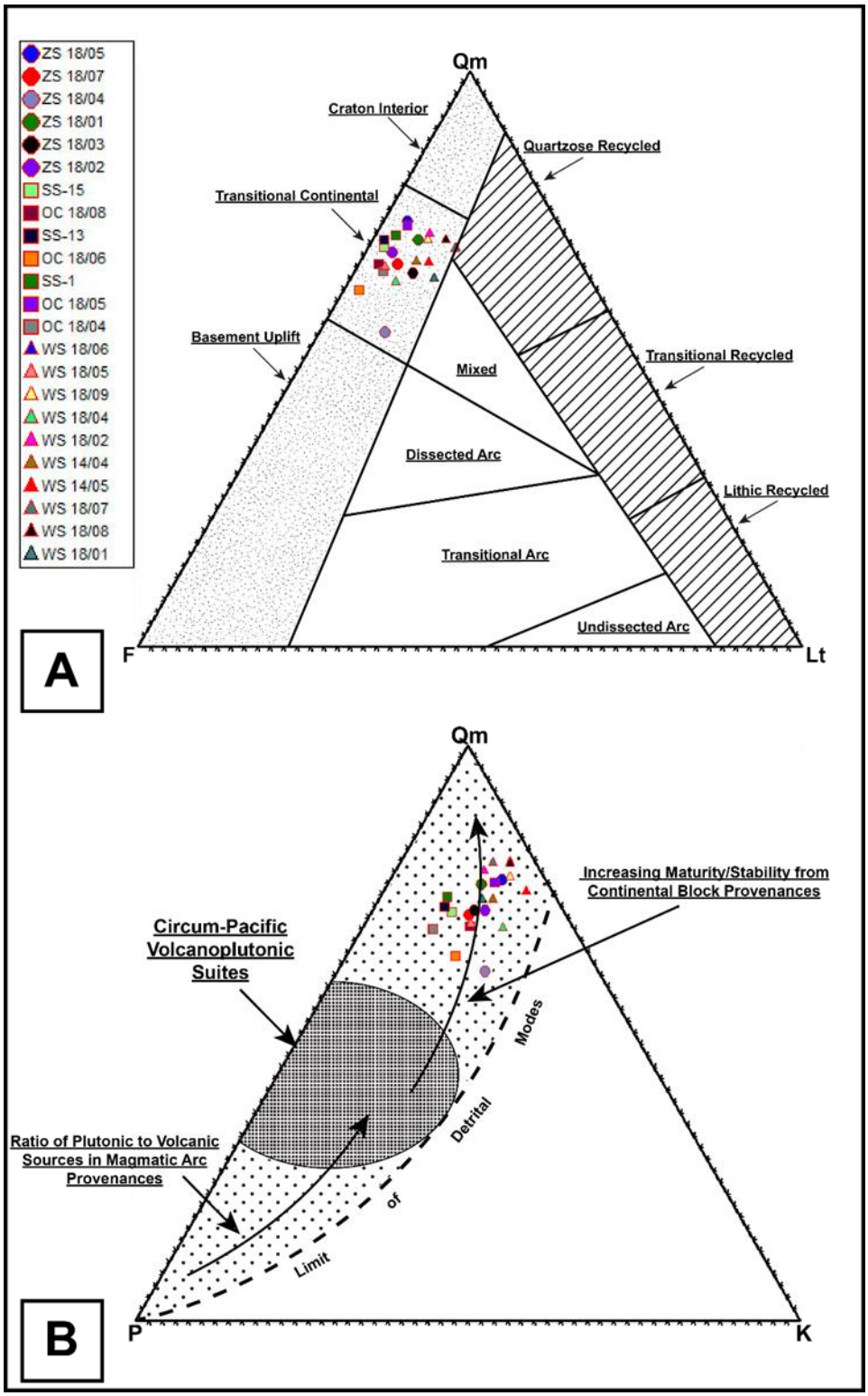

Figure 10: A.) Qm-F-Lt ternary plot using the classification scheme developed by Dickinson (1985) for provenance analysis. **B.)** Qm-P-K ternary plot using the classification scheme developed by Dickinson (1985) for provenance analysis.

Chapter 5: Discussion

Provenance of the Moenave Formation

Detrital Zircon U-Pb Ages

Comparison of composite detrital zircon U-Pb age distributions (Fig. 11) and petrographic analyses (Fig. 12) from the Moenave Formation and surrounding stratigraphic units reveals the differences and similarities in age spectrums and grain composition that helps illuminate the sediment provenance and clarify the paleogeographic story of the Moenave Formation. Surrounding stratigraphic units in this comparison consist of the Chinle Formation (Dickinson and Gehrels, 2008; Marsh et al., 2019), the Wingate Sandstone, the Springdale Sandstone, the Kayenta Formation, and the Navajo Sandstone (Dickinson and Gehrels, 2009a). Excluding the Springdale Sandstone sample, observations of the composite detrital zircon U-Pb age distributions show that heterogeneous age populations of pre-Appalachian derived grains (greater than 800 Ma) are broadly similar (Fig. 11).

Chinle Formation

The Chinle Formation data was selected to represent the regional paleogeography related to the Moenave sample site locations, consisting of samples from the lower Chinle paleodrainage system west of the Rio Grande rift (Dickinson and Gehrels, 2008). Compared to the detrital zircon U-Pb relative age distribution (Fig. 11) of the Moenave Formation (n=5145), the Chinle Formation (n=892) in this region exhibits age populations similar to the Moenave Formation with the exception of the lack of Paleozoic and Neoproterozoic Appalachian grains. A broad range of Grenville ages are present in both formations, while significantly more pronounced age peaks of the Cordilleran magmatic arc and Mesoproterozoic anorogenic plutons are present within the age

distribution of the Chinle Formation, indicative of south and southeastern tributaries supplying sediment to the northwest flowing lower Chinle fluvial system (Dickinson and Gehrels, 2008).

Wingate Sandstone

Similarity in age populations of pre-Cordilleran magmatic arc grains can be observed between the Wingate Sandstone (*n*=103) and the Moenave Formation, with the complete absence of Cordilleran arc grains in the Wingate Sandstone being the defining difference (Fig. 11). Paleowind measurements within Jurassic ergs show a southward blowing wind, indicating a northern source of sediment. From those measurements, Dickinson and Gehrels (2009a) inferred that sediment was transported by a northwest flowing transcontinental Jurassic paleoriver system that transported sediment from the central and southern Appalachians to Jurassic paleoshorelines north of the Colorado Plateau, which was then transported to Jurassic ergs by the south blowing winds. The headwaters of this paleoriver provided Appalachian and Grenville derived grains, while southern tributaries supplied sediment from Yavapai-Mazatzal basement intruded by anorogenic plutons east of the Colorado Plateau (Dickinson and Gehrels, 2009a). The absence of Cordilleran arc grains and southward blowing paleowinds implies Wingate Sandstone sediment was not sourced south of the Colorado Plateau.

Springdale Sandstone

The Springdale Sandstone (*n*=94) lacks Appalachian and Yavapai-Mazatzal derived grains and consists mainly of Cordilleran arc derived grains, a less broad distribution of Grenville derived grains, and a small input of Yavapai-Mazatzal grains (Fig. 11). The abundance of arc derived grains in the Springdale Sandstone, with the absence of any Appalachian grains, suggests derivation from southwest Laurentia positioned directly to the south from Springdale exposures in

Mexico where Grenville terranes are present, mixing sediment with arc-derived Cordilleran detritus (Dickinson and Gehrels, 2009a).

Kayenta Formation

The Kayenta Formation (*n*=250) age spectra are most similar to the Moenave Formation cumulative age distributions (Fig. 11), suggesting that the Kayenta Formation follows close to the same trend as the Moenave Formation apart from the Neoproterozoic Appalachian age range. Pre-Appalachian age populations (greater than 800 Ma) are similar. The Kayenta Formation exhibits both Paleozoic (406 Ma) and Neoproterozoic (589 Ma) age peaks with the latter having a lower abundance of grains compared to the Moenave Formation. Cordilleran arc derived grains within the composite age distribution of the Kayenta Formation show age peaks within the range of 288-231 Ma suggesting a southeastern source indicative of the East Mexico arc (284-232 Ma), however the most southwestern Kayenta sample, closest to this study's sample locations, contains arc derived grains with an age peak of 231 Ma suggesting a younger Cordilleran arc (younger than 241 Ma) southern source (Dickinson and Gehrels, 2009a). Arc-derived grains being sourced from the south can provide an explanation for the presence of Yavapai-Mazatzal basement and Mesoproterozoic anorogenic pluton grains, most likely sharing a fluvial pathway. Furthermore, Dickinson and Gehrels (2009a) interpreted Appalachian and Grenville derived grains being contributed by redistributed eolian sands from underlying unconsolidated erg deposits.

Navajo Sandstone

Similarity in age populations of pre-Cordilleran magmatic arc grains can be observed between the Navajo Sandstone (n=195) and the Moenave Formation, with the complete absence of Cordilleran arc grains in the Navajo Sandstone being the defining difference (Fig. 11). Navajo

Sandstone sediment dispersal follows a similar pattern to the Wingate Sandstone dispersal pathways.

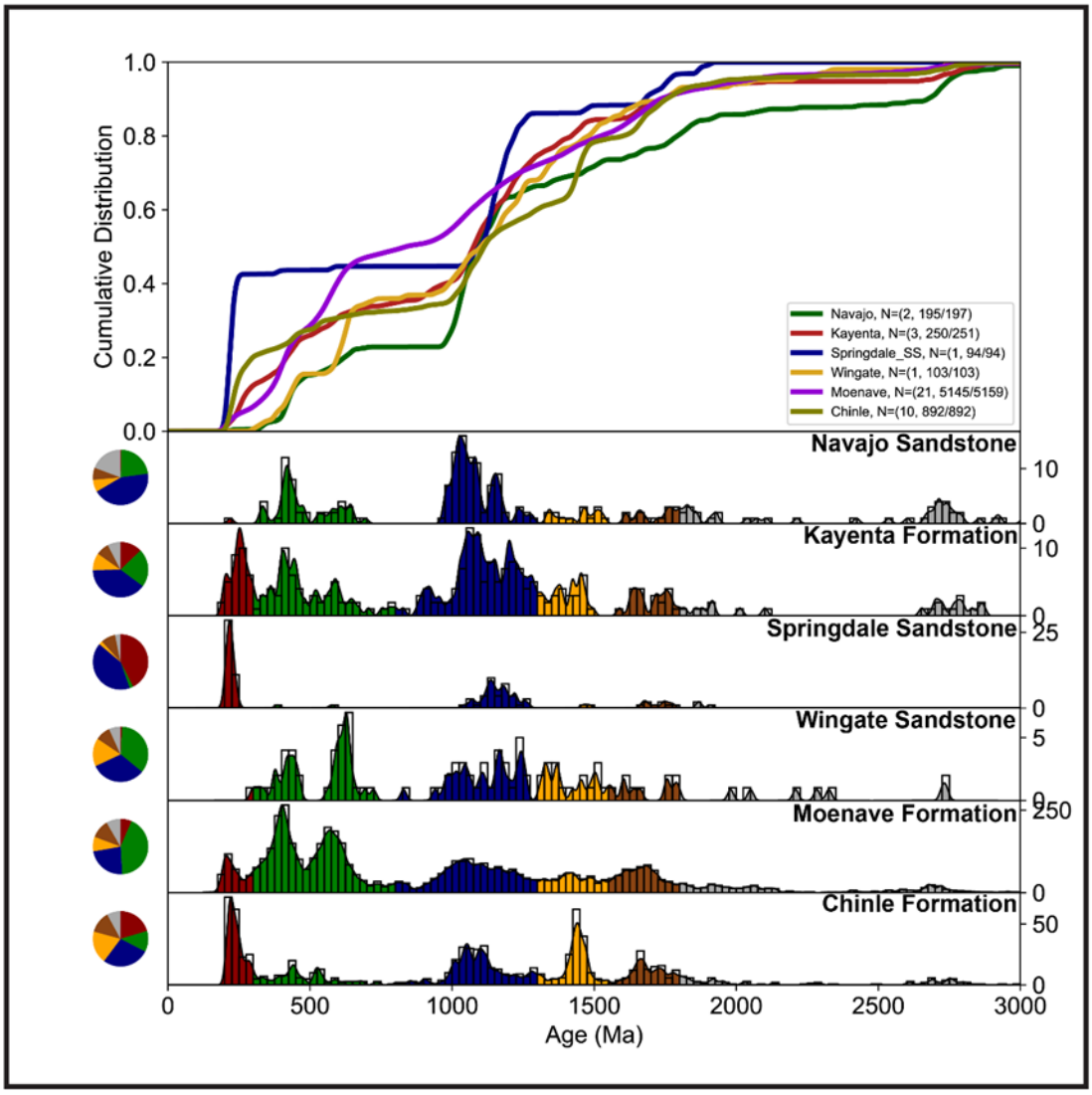

Figure 11: Detrital zircon U-Pb age distributions (0-3000 Ma) from this study and previously published samples. Data is grouped into lithostratigraphic units. Distributions are cumulative (top) and relative (bottom) KDEs of sample groups with a bandwidth of 10 Myr. Pie charts are reported to visualize percent abundance of age populations. Coloring corresponds with the map of North American basement provinces and their crystallization age (Fig. 1). Chinle Formation data are provided by Dickinson and Gehrels, (2008) and Marsh et al. (2019). Wingate Sandstone, Springdale Sandstone, Kayenta Formation, and Navajo Sandstone data are provided by Dickinson and Gehrels (2009a).

Petrographic Analysis Comparison

Petrographic analysis serves as an alternative method to detrital zircon U-Pb age distributions and an extra source of information for provenance interpretation. This study compares detrital modes clustered into corresponding formations with the exception of Jurassic eolianites for which multiple formations are clustered into a single group. The Chinle Formation and the Chinle-Dockum group detrital mode samples are taken from Dickinson and Gehrels (2008) and the Kayenta Formation and Jurassic eolianite samples are taken from Dickinson and Gehrels (2009a). Detrital modes are plotted on a Qm-F-Lt ternary diagram using the classification scheme of Dickinson (1985) to provide a graphical representation of different tectonic settings of provenance type (Fig. 12). Visual inspection of the provenance ternary diagram shows quartzose rich Jurassic eolianites are tightly clustered within the provenance terrane classification of craton interior. Chinle and Chinle-Dockum detrital modes plot in an elongate cluster encompassing both the craton interior and quartzose recycled provenance terrane classifications due to a more quartzoselithic composition within the samples. Interestingly, the quartzosefeldspathic Kayenta sample cluster plots in concordance with the quartzosefeldspathic Moenave cluster, falling under the transitional continental provenance terrane classification, characterized by the transition between craton interior and basement uplift. This shared provenance type reveals that the Moenave Formation and Kayenta Formation share similar detrital composition (Dickinson, 1985), which correlates well with the strong similarities between the detrital zircon U-Pb age distributions of these two formations.

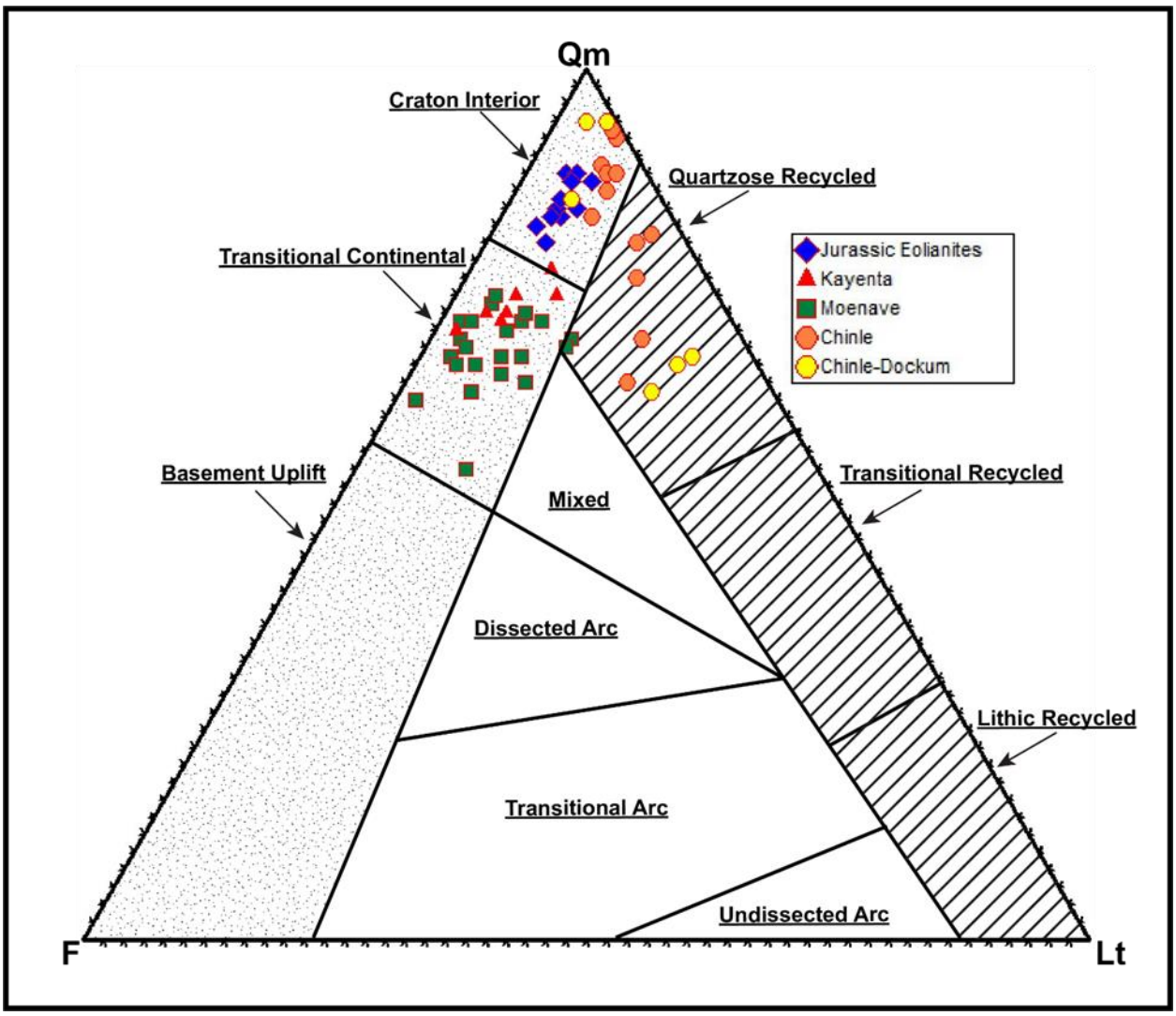

Figure 12: Qm-F-Lt ternary plot using the classification scheme developed by Dickinson (1985) for provenance analysis. Detrital modes plotted are from this study and previously published samples. Chinle and Chinle-Dockum data are provided by Dickinson and Gehrels, (2008). Kayenta and Jurassic Eolianites data are provided by Dickinson and Gehrels, (2009a).

Provenance Interpretation

Earlier interpretations of the provenance of the Moenave have described the sediment sources and sediment dispersal pathways using only stratigraphic and sedimentologic information. Paleocurrent indicators show that Early Jurassic river systems preserved in the DCM flowed from the southeast to the northwest along the Zuni sag, transporting sediment largely derived from the south (Mogollan slope) and the east (Riggs and Blakey, 1993; Blakey, 1994; Tanner and Lucas, 2009; Kirkland et al., 2014). Eolian crossbedding preserved in the Wingate and Navajo Sandstones indicates that wind blew sand toward the southeast (Clemmensen and Blakey, 1989; Clemmensen et al., 1989). Interpreted models show resultant paleowinds from the northwest blew fluvial sand from a transcontinental paleoriver, terminated northwest of the Colorado Plateau, into the adjacent part of the Wingate erg, where a portion would be reworked into the Moenave paleorivers flowing back toward the northwest. Also, due to deflation a portion of Moenave fluvial sediment would then be reworked back into the erg by prevailing westerly winds (Clemmensen and Blakey, 1989; Blakey, 1994; Dickinson and Gehrels, 2003; Dickinson and Gehrels 2009a; Tanner and Lucas, 2009). All interpretations contribute to the Moenave Formation being a northwest trending fluviolacustrine system having sediment supplied from the south derived from the Mogollan slope, the southeast derived from the Cordilleran magmatic arc, and further contribution from reworked sediment derived from erg deposits. However, that agreement is established on a complete absence of detrital zircon U-Pb age distributions and petrographic analyses of the Moenave Formation.

This study proposes to use the provenance interpretation of the Kayenta Formation from Dickinson and Gehrels (2009a) as an analogue for the Moenave Formation. Evaluating the evidence that supports the strong similarities between the Moenave Formation and the Kayenta Formation, provided by the comparison of composite detrital zircon U-Pb relative and cumulative

age distributions (Fig. 11) and petrographic analyses (Fig. 12). The Cordilleran magmatic arc age population present within the Moenave has a dominant age peak of 206 Ma indicating that grains were derived from the southeast portion (near southwestern New Mexico) of the younger Cordilleran arc rather than the older East Mexico arc. Appalachian, Grenville, and older north Laurentia (1800 Ma and older) grains were likely derived from reworked sediment of the adjacent Wingate erg. A northwest flowing transcontinental paleoriver with headwaters in central Appalachian province transported sediment north of the Colorado Plateau to early Jurassic paleoshorelines where southeast blowing paleowinds transported this sediment to supply the Wingate erg, which was then reworked into Moenave fluvial system. However, petrographic analysis shows the erg deposits are too quartz rich compared to the abundance of feldspars in the Moenave, which suggests that the sediment reworked from the adjacent Wingate erg was a minor source for the Moenave. Grains derived from Yavapai-Mazatzal basement and associated Mesoproterozoic plutons were likely derived from the Mogollan slope to the south. Resulting sediment dispersal pathways of the Moenave northwest trending fluvial system along the Zuni sag consist of tributaries from the north and northeast representing the redistribution of eolian sands, tributaries from the south carrying feldspathic sand and silt derived from the Mogollan slope and a sediment source representing Appalachian and Grenville detritus, and tributaries from the southeast representing sediment delivery from the Cordilleran magmatic arc. Furthermore, observations from individual detrital zircon U-Pb age distributions of Moenave samples (Fig. 6) show a correlation between Cordilleran arc and Yavapai-Mazatzal age abundances, indicating that tributaries from the south and southeast may have combined into one contributing system. Thus, although the present findings for the Moenave Formation are in agreement with existing

interpretations, the inclusion of detrital zircon U-Pb geochronology and sandstone petrography provides a new level of insights into sediment routing patterns during this time.

Maximum Depositional Age of the Moenave Formation

Chronostratigraphic Constraints

Previous interpretations of the age of the Moenave Formation have estimated it to be late Triassic (Rhaetian) to Early Jurassic (Hettangian) in age (~200-196 Ma) (Tanner and Lucas, 2009; Milner et al., 2012; Kirkland et al., 2014; Suarez et al., 2017). Our detrital zircon U-Pb data are significant in that they have abundant zircons circa 200 Ma, which shows that the Moenave is definitively latest Triassic or younger. Debate over whether the basal Moenave is late Triassic or if the TJB is lost within the J-0 unconformity has been discussed by Milner et al. (2012) and Kirkland et al. (2014). If the basal Moenave is late Triassic in age, this would mean the TJB (201.3 ± 0.2 Ma.; Hillebrandt et al., 2013) falls somewhere within the Moenave Formation. Detrital zircon ages determined by LA-ICP-MS have proven difficult to pinpoint the exact stratigraphic position of the ETE and TJB due to relatively high analytical uncertainty (~ 3.0 Ma 2σ % error for young Cordilleran grains) as well as anomalously young grains at the basal DCM (Willow Springs and Blacks Canyon) and towards the top of the DCM (Willow Springs) (Table 6). Sample ZS 18/07 YSG has an age of 190.6 ± 4.5 Ma and sample WS 14/02 YSG has an age of 192.5 ± 7.1 Ma. The YSG at the uppermost WPM sample at Olsen Canyon has an age of 139.7 ± 3.7 Ma with the next youngest grain with an age of 177.3 ± 2.6 Ma. These youngest grains, however, are isolated and anomalous. The YSG for the basal DCM sample, OC 18/02, at the Olsen Canyon section is 203.8 ± 5.7 Ma, designating a Rhaetian age or younger, and the YSG for the upper WPM sample, ZS

18/05, at the Blacks Canyon section is 197 ± 4.5 Ma, designating a Hettangian age or younger. These two samples provide a limited interpretation for chronostratigraphic constraints, because single grain ages can be affected by Pb loss, other analytical defects, or contamination. Therefore, clusters of at least two or more grains are used for MDA analysis.

Placement of the ETE

Figure 7 shows individual sample MDA calculations with stratigraphic height vs. age plots in comparison with the determined ETE age (201.564 ± 0.015 Ma; Blackburn et al., 2013). Added to the Blacks Canyon plot is the CA-ID-TIMS age (201.28 ± 0.11/0.15 Ma) collected from the middle WPM by Suarez et al. (2017) for reference. Visual inspection of the MDA stratigraphic height vs. age plots shows a slight upward younging in each section. For constraining the placement for the ETE in each section, this study will use an aggregate of conservative MDA estimates (YC2σ, Y3Zo, YSP, τ method), due to the absence of high precision data. This study focuses on the stratigraphically lowest occurrence of clustered conservative MDA estimates that are younger than the ETE, suggesting the ETE is below these lowest occurring clusters. Sample ZS 18/01 from the lower-middle DCM in the Blacks Canyon section, sample OC 18/06 from the middle DCM in the Olsen Canyon section, and sample WS 18/05 from the lower-middle DCM in the Willow Springs section contain the lowest occurrence of clustered conservative MDA estimates that are younger than (within 2σ uncertainty) the ETE (Fig. 7), suggesting the ETE, if present, is within the lower DCM. To summarize, all three studied sections yield conservative MDA estimates that are consistent with the ETE, if present, being located in the lower DCM.

Future Work

For future work, the youngest grains will be processed for CA-ID-TIMS. Table 9 provides a list of proposed detrital zircon grains to be processed. Before selection, grains were filtered for discordance (between -5% and 5%) and uranium concentration (<1000 ppm). This will provide invaluable information and will likely improve the precision of the maximum depositional age of each sample and for the Moenave Formation overall. Furthermore, these high precision data will provide a clearer answer to the placement of the ETE contributing a valuable low latitude record of the climatic and biotic changes associated with Central Atlantic Magmatic Province.

Table 9: Proposed Detrital Zircon Grains for CA-ID-TIMS

Sample Grain ID	Best Age (Ma)	Error 2σ (Ma)	Discordance (-5%-5%)	U ppm (<1000)
Willow Springs				
WS 1809.B.142	177.4	2.1	2.0	243
WS 1809.B.129	189.8	4.6	2.2	153.7
WS 1808.127	191.3	3.5	3.4	324
WS 1808.B.50	191.5	3.2	1.5	455
WS 1808.114	199.4	3.2	2.3	176.7
WS 1808.106	200.5	4.1	1.7	57.8
WS 1805.B.59	194	3.4	0	130.7
WS 1805.02	196.4	2.45	4.2	368
WS 1805.B.135	197	5.5	1.0	153.5
WS 1403.B.94	197.8	2.7	-1.3	591
WS 1403.B.131	200.8	2.3	4.2	621
WS 1403.B.150	201	3.2	-1.5	215
WS 1403.B.132	204	2.6	-0.3	410
WS 1402.B.52	192.5	3.6	2.3	224
Blacks Canyon				
ZS 1805.20	197	2.3	1.0	201.8
ZS 1804.126	188	5.5	0.5	443
ZS 1804.B.60	196.6	4.0	-1.9	228
ZS 1803.B.81	201	3.7	2.9	294.6
ZS 1504.B.41	196.2	3.3	-1.1	302
ZS 1504.51	201.9	1.9	1.9	834
ZS 1504.97	203.8	2.3	0.1	140.8
ZS 1802.B.77	197.5	3.5	3.2	577
ZS 1802.61	200.1	3.3	1.8	958
ZS 1802.B.110	201.8	3.0	2.0	454
ZS 1802.135	203.5	2.4	1.9	689
ZS 1801.143	185	4.7	3.6	307
ZS 1801.58	191.2	2.2	3.1	792
ZS 1801.104	197.1	2.6	-0.6	493
ZS 1801.B.132	198.8	4.3	3.5	424

Table 9: Proposed Detrital Zircon Grains for CA-ID-TIMS Cont.

Sample Grain ID	Best Age (Ma)	Error 2σ (Ma)	Discordance (-5%-5%)	U ppm (<1000)
Blacks Canyon				
ZS 1503.B.37	198	5.5	4.3	118.6
ZS 1503.116	198.6	3.9	-3.4	176.1
ZS 1503.15	199.9	3.55	4.81	435
ZS 1503.B.97	203	2.5	1.5	290
ZS 1503.91	203.5	1.9	-2.5	719
ZS 1503.10	204.9	3.35	0.53	208.5
ZS 1807.B.145	190.6	2.3	-0.3	361
Olsen Canyon				
OC 1808.B.46	177.3	2.6	0.4	496
OC 1808.07	198.3	2.4	-2.1	476
OC 1808.30	201	1.9	-0.6	355
OC 1807.B.82	189.8	2.8	2.2	458
OC 1807.B.38	196.7	3.3	0.2	509
OC 1807.131	203.2	2.55	4.6	209
OC 1806.B.126	193.1	3.1	3.9	316
OC 1806.2.41	196	2.2	-1.66	334
OC 1806.B.75	201.9	3.2	1.5	329.2
OC 1806.B.66	202	5.5	-1.5	355
OC 1805.60	200.7	1.95	2.86	750
OC 1805.16	200.9	1.75	3.69	675
OC 1804.107	202.2	2.1	-0.1	336
OC 1803.23	201.1	2.8	-1.57	294.8
OC 1802.15	203.8	2.85	4.32	721

Chapter 6: Conclusions

Although the underlying Chinle Formation and overlying Kayenta Formation have been extensively sampled for detrital zircon geochronology (e.g., Dickinson et al., 2008; 2009a; Marsh et al., 2019), the provenance of the Moenave Formation is poorly documented with only two known published samples from Suarez et al. (2017) with a limited sample size (93 grain analyses). This preliminary data suggested that the Moenave Formation may have distinct detrital zircon U-Pb age spectra relative to surrounding stratigraphic units (Suarez et al., 2017). Detrital zircon U-Pb age distributions and petrographic analyses presented here show strong similarities in the sediment composition and dispersal pathways between the Moenave Formation and the Kayenta Formation. This study uses the model laid out by Dickinson and Gehrels (2009a) to characterize the provenance of the Moenave Formation along with further interpretation of unique Moenave age spectra and sediment composition. Resulting sediment dispersal pathways of the Moenave northwest trending fluvial system along the Zuni sag consist of tributaries from the north and northeast representing the minor redistribution of eolian sands, tributaries from the south representing the Mogollan slope and feldspar rich detritus from Appalachian and Grenville sources, and tributaries from the southeast representing sediment delivery from the Cordilleran magmatic arc. Furthermore, detrital zircon U-Pb age distributions show a correlation between Cordilleran arc and Yavapai-Mazatzal age abundances, indicating that tributaries from the south and southeast may have combined into one contributing system. The present findings for the provenance of the Moenave Formation using detrital zircon U-Pb geochronology and sandstone petrography are in agreement with existing interpretations but paint a clearer picture of the Moenave sediment routing system. Furthermore, the study aimed constrain TJB and ETE stratigraphic positions by applying nine different maximum depositional age (MDA) calculations

from the resulting detrital zircon U-Pb laser ablation data using methods outlined by Coutts et al. (2019). An abundance of zircons circa 200 Ma definitively constrains the Moenave Formation to be latest Triassic or younger in age. Due to relatively wide ranges in uncertainty (~ 3.0 Ma 2σ % error for young Cordilleran grains), determining age constraints and placement of the ETE is difficult. Using a conservative approach, this study chose to use an aggregate of conservative MDA estimates based on clusters of grain ages (YC2σ, Y3Zo, YSP, and the τ method), rather than rely on single youngest grain ages. Within each section, clustered conservative MDA estimates show that the Moenave becomes younger than the ETE within the lower-middle and middle DCM, constraining the ETE, if present, to the lower DCM.

References

Antonietto, L. S., Boush, L. E., Suarez, C. A., Milner, A. R., & Kirkland, J. I. (2018). The 'Last Hurrah of the Reigning Darwinulocopines'? Ostracoda (Arthropoda, Crustacea) from the Lower Jurassic Moenave Formation, Arizona and Utah, USA. Journal of Paleontology, 92(4), 648-660.

Barbeau, D. L., Olivero, E. B., Swanson-Hysell, N. L., Zahid, K. M., Murray, K. E., & Gehrels, G. E. (2009). Detrital-zircon geochronology of the eastern Magallanes foreland basin: Implications for Eocene kinematics of the northern Scotia Arc and Drake Passage. Earth and Planetary Science Letters, 284(3-4), 489-503.

Black, L. P., Kamo, S. L., Allen, C. M., Davis, D. W., Aleinikoff, J. N., Valley, J.W., Mundil, R., Campbell, I.H., Korsch, R.J., Williams, I.S., Foudoulis, C. (2004). Improved 206Pb/238U microprobe geochronology by the monitoring of a trace-element-related matrix effect; SHRIMP, ID–TIMS, ELA–ICP–MS and oxygen isotope documentation for a series of zircon standards. Chemical Geology, 205(1-2), 115-140.

Blackburn, T., Olsen, P.E., Bowring, S.A., McLean, N.M., Kent, D.V., Puffer, J., McHone, G., Rasbury, E.T., Et-Touhami, M. (2013). Zircon U–Pb geochronology links the end-Triassic extinction with the Central Atlantic Magmatic Province. Science

Blakey, R.C., (1994). Paleogeographic and tectonic controls on some Lower and Middle Jurassic erg deposits, Colorado Plateau, in Caputo, M.V., Peterson, J.A., Franczyk, J.J., (eds.), Mesozoic systems of the Rocky Mountain region, USA: Rocky Mountain Section, Society of Economic Paleontologists and Mineralogists, Special Publication, p. 273-298. Blakey, R. L., & Ranney, W. (2008). Ancient landscapes of the Colorado Plateau. Grand Canyon, AZ: Grand Canyon Association.

Clemmensen, L.R., Blakey, R.L. (1989). Erg deposits of the Lower Jurassic Wingate Sandstone: oblique dune sedimentation. Sedimentology 36, 449–470.

Clemmensen, L. R., Olsen, H., & Blakey, R. L. (1989). Erg-margin deposits in the Lower Jurassic Moenave Formation and Wingate Sandstone, southern Utah. Geological Society of America Bulletin, 101(6), 759-773.

Coutts, D. S., Matthews, W. A., & Hubbard, S. M. (2019). Assessment of widely used methods to derive depositional ages from detrital zircon populations. Geoscience Frontiers, 10(4), 1421-1435.

Dickinson, W.R. and Suczek, C.A. (1979) Plate Tectonics and Sandstone Compositions. American Association of Petroleum Geologists' Bulletin, 63, 2164-2182.

Dickinson, W. R. (1985). Interpreting Provenance Relations from Detrital Modes of Sandstones. Provenance of Arenites, 333-361.

Dickinson, W. R. (2009). Anatomy and global context of the North American Cordillera. Backbone of the Americas: Shallow Subduction, Plateau Uplift, and Ridge and Terrane Collision.

Dickinson, W. R., & Gehrels, G. E. (2003). U–Pb ages of detrital zircons from Permian and Jurassic eolian sandstones of the Colorado Plateau, USA: Paleogeographic implications. Sedimentary Geology, 163(1-2), 29-66.

Dickinson, W. R., & Gehrels, G. E. (2008). U-Pb Ages of Detrital Zircons in Relation to Paleogeography: Triassic Paleodrainage Networks and Sediment Dispersal Across Southwest Laurentia. Journal of Sedimentary Research, 78(12), 745-764.

Dickinson, W. R., & Gehrels, G. E. (2009a). U-Pb ages of detrital zircons in Jurassic eolian and associated sandstones of the Colorado Plateau: Evidence for transcontinental dispersal and intraregional recycling of sediment. Geological Society of America Bulletin, 121(3-4), 408-433.

Dickinson, W.R., and Gehrels, G.E. (2009b). Use of U-Pb ages of detrital zircons to infer maximum deposition ages of strata: A test against a Colorado Plateau Mesozoic database: Earth and Planetary Science Letters, v. 288, p. 115-125.

Donohoo-Hurley, L.L., Geissman, J.W., Lucas, S.G., Kuerschner, W. (2009). The Triassic/Jurassic boundary, Colorado Plateau area, USA: magnetostratigraphic correlation of theMoenave Formation with the strata from the St. Audrie's Bay, UK, Morocco, andNewark/Hartford basins. Geological Society of America Abstracts with Programs 41 (7), 182.

Donohoo-Hurley, L. L., Geissman, J. W., & Lucas, S. G. (2010). Magnetostratigraphy of the uppermost Triassic and lowermost Jurassic Moenave Formation, western United States: Correlation with strata in the United Kingdom, Morocco, Turkey, Italy, and eastern United States. Geological Society of America Bulletin, 122(11-12), 2005-2019.

Downs, D.T. (2009). In search of the Triassic-Jurassic boundary—palynostratigraphy and carbon-isotope stratigraphy of the lower Dinosaur Canyon Member on the Colorado Plateau (Kanab, Utah): Carbondale, Illinois, Southern Illinois University, M.S. thesis, 116 p.

Fildani, A., McKay, M., Stockli, D., Clark, J., Dykstra, M., Stockli, L., & Hessler, A. (2016). The ancestral Mississippi drainage archived in the late Wisconsin Mississippi deep-sea fan. Geology, 44(6), 479-482.

Folk, R.L. (1968 and 1980). Petrology of Sedimentary Rocks. Austin (USA), Hemphill Publishing Co., 182 p.

Gehrels, G. (2014). Detrital Zircon U-Pb Geochronology Applied to Tectonics. Annual Review of Earth and Planetary Sciences, 42(1), 127-149.

Guex, J., Bartolini, A., Atudorei, V., Taylor, D. (2014). High-resolution ammonite and carbon isotope stratigraphy across the Triassic–Jurassic boundary at New York Canyon (Nevada). Earth Planet. Sci. Lett. 225, 29–41.

Harshbarger, J.W., Repenning, C.A., Irwin, J.H. (1957). Stratigraphy of the uppermost Triassic and the Jurassic rocks of the Navajo Country. U. S. Geological Survey Professional Paper 291, 12–26.

Hesselbo, S.P., Robinson, S.A., Surlyk, F., Piasecki, S. (2002). Terrestrial and marine extinction at the Triassic-Jurassic boundary synchronized with major carbon-cycle perturbation: A link to initiation of massive volcanism? Geology 30, 251–254.

Houghton, H. F. (1980). Refined techniques for staining plagioclase and alkali feldspars in thin section. Journal of Sedimentary Research, 50(2), 629-631.

Kirkland, J. I., Milner, A. C., Olsen, P. E., & Hargrave, J. E. (2014). The Whitmore Point Member of the Moenave Formation in its type area in Northern Arizona and its age and correlation with the section in St. George, Utah: evidence for two major lacustrine sequences. Geology of Utah's Far South: Utah Geological Association Publication, 43, 321-356.

Lucas, S., Tanner, L., Donohoo-Hurley, L., Geissman, J., Kozur, H., Heckert, A., & Weems, R. (2011). Position of the Triassic–Jurassic boundary and timing of the end-Triassic extinctions on land: Data from the Moenave Formation on the southern Colorado Plateau, USA. Palaeogeography, Palaeoclimatology, Palaeoecology,302(3-4), 194-205.

Marsh Thesis (2019) Constraining the age of the Kayenta Formation using U-Pb detrital zircon geochronology from lithostratigraphic sections and vertebrate fossil localities in Arizona and Utah

Marsh, A. D., Parker, W. G., Stockli, D. F., & Martz, J. W. (2019). Regional correlation of the Sonsela Member (Upper Triassic Chinle Formation) and detrital U-Pb zircon data from the Sonsela Sandstone bed near the Sonsela Buttes, northeastern Arizona, USA, support the presence of a distributive fluvial system. Geosphere.

Marzolf, J.E. (1994). Reconstruction of the early Mesozoic Cordilleran cratonic margin adjacent to the Colorado Plateau. In: Caputo, M.V., Peterson, J.A., Franczyk, K.J. (Eds.), Mesozoic Systems of the Rocky Mountain Region, USA. Rocky Mountain Section SEPM, Denver, pp. 181–215.

Marzoli, A., Renne, P.R., Piccirillo, E.M., Ernesto, M., Bellieni, G., De Min, A. (1999), Extensive 200-million-year-old continental flood basalts of the Central Atlantic Magmatic Province: Science, v. 284, p. 616–618.

Mcbride, E. F. (1963). A Classification of Common Sandstones. SEPM Journal of Sedimentary Research, Vol. 33.

Milner, Andrew & Birthisel, Tylor & Kirkland, James & H. Breithaupt, Brent & Matthews, Neffra & Lockley, Martin & Santucci, Vincent & Z. Gibson, Sarah & DeBlieux, Donald & Hurlbut, Melinda & Harris, Jerry & Olsen, Paul. (2012). Tracking Early Jurassic dinosaurs across southwestern Utah and the Triassic-Jurassic Transition. Nevada State Museum Paleontological Papers. 1. 1-107.

Oefinger, Jordan (unpublished)

Olsen, H. (1989). Sandstone-body structures and ephemeral stream processes in the Dinosaur Canyon Member, Moenave Formation (Lower Jurassic), Utah, U.S.A. Sedimentary Geology 61, 207–221.

Paton, C., Hellstrom, J., Paul, B., Woodhead, J., & Hergt, J. (2011). Iolite: Freeware for the visualisation and processing of mass spectrometric data. Journal of Analytical Atomic Spectrometry, 26(12), 2508.

Petrus, J. A., & Kamber, B. S. (2012). VizualAge: A Novel Approach to Laser Ablation ICP-MS U-Pb Geochronology Data Reduction. Geostandards and Geoanalytical Research, 36(3), 247-270.

Pipiringos, G., & Osullivan, R. B. (1978). Principal unconformities in Triassic and Jurassic rocks, western interior United States; a preliminary survey. Professional Paper.

Riggs, N. R., Lehman, T. M., Gehrels, G. E., & Dickinson, W. R. (1996). Detrital Zircon Link Between Headwaters and Terminus of the Upper Triassic Chinle-Dockum Paleoriver System. Science, 273(5271), 97-100.

Riggs, N.R., and Blakey, R.C., (1993). Early and Middle Jurassic paleogeography and volcanology of Arizona and adjacent areas: Society of Economic Paleontology and Mineralogy, Pacific Section, Mesozoic Paleogeography, Book 71, p. 347- 375.

Ross, J. B., Ludvigson, G. A., Möller, A., Gonzalez, L. A., & Walker, J. D. (2016). Stable isotope paleohydrology and chemostratigraphy of the Albian Wayan Formation from the wedge-top depozone, North American Western Interior Basin. Science China Earth Sciences, 60(1), 44-57.

Schaller, M.F., Wright, J.D., Kent, D.V. (2015). A 30 Myr record of Late Triassic atmospheric pCO2 variation reflects a fundamental control of the carbon cycle by changes in continental weathering. Geol. Soc. Am. Bull. 127, 661–671.

Schoene, B., Guex, J., Bartolini, A., Schaltegger, U., Blackburn, T.J. (2010). Correlating the end-Triassic mass extinction and flood basalt volcanism at the 100 ka level. Geology 38, 387–390.

Sharman, G. R., Sharman, J. P., & Sylvester, Z. (2018). DetritalPy: A Python-based toolset for visualizing and analysing detrital geo-thermochronologic data. The Depositional Record, 4(2), 202-215.

Sharman, G.R., Stockli, D.F., Flaig, P., Raynolds, R.G., and Covault, J.A., (2018). Local-to-distant sediment source area cyclicity of the southern Front Range, central Colorado: Insights from detrital zircon geochronology, in, Ingersoll, R.V., Lawton, T.F., and Graham, S.A., Tectonics, Sedimentary Basins, and Provenance: A Celebration of the Career of William R. Dickinson, Geological Society of America Special Paper 540

Slama, J., Košler, J., Condon, D.J., Crowley, J.L., Gerdes, A.E., Hanchar, J.M., Horstwood, M.S., Morris, G.A., Nasdala, L., Norberg, N.S., Schaltegger, U., Schoene, B., Tubrett, M., & Whitehouse, M.J. (2008). Plešovice zircon: a new natural reference material for U-Pb and Hf isotopic microanalysis.

Steiner, M. (2014). New magnetostratigraphy and paleopole from the Whitmore Point Member of the Moenave Formation at Kanab, Utah.

Suarez, C. A., Knobbe, T. K., Crowley, J. L., Kirkland, J. I., & Milner, A. R. (2017). A chronostratigraphic assessment of the Moenave Formation, USA using C-isotope

chemostratigraphy and detrital zircon geochronology: Implications for the terrestrial end Triassic extinction. Earth and Planetary Science Letters,475, 83-93.

Tanner, L. H., & Lucas, S. G. (2007). The Moenave Formation: Sedimentologic and stratigraphic context of the Triassic–Jurassic boundary in the Four Corners area, southwestern U.S.A. Palaeogeography, Palaeoclimatology, Palaeoecology, 244(1-4), 111-125.

Tanner, L. H., & Lucas, S. G. (2009). The Whitmore Point Member of the Moenave Formation: Early Jurassic Dryland Lakes on the Colorado Plateau, Southwestern USA. Volumina Jurassica, 6(6), 11-21.

Tanner, L. H., & Lucas, S. G. (2010). Deposition and deformation of fluvial–lacustrine sediments of the Upper Triassic–Lower Jurassic Whitmore Point Member, Moenave Formation, northern Arizona. Sedimentary Geology, 223(1-2), 180-191.

Thompson, T. (2009). TriPlot Ternary plotting software

Whiteside, J.H., Olsen, P.E., Eglinton, T., Brookfield, M.E., Sambrotto, R.N. (2010). Compound-specific carbon isotopes from Earth's largest flood basalt eruptions directly linked to the end-Triassic mass extinction. Proc. Natl. Acad. Sci. 107, 6721–6725.

Wiedenbeck, M., Allé, P., Corfu, F., Griffin, W.L., Meier, M., Oberli, F., von Quadt, A., Roddick, J.C. and Spiegel, W. (1995). Three natural zircon standards for U-Th-Pb, Lu-Hf, trace element and REE analyses. Geostandards Newsletter, 19, 1-23

Zhang, X., Pease, V., Skogseid, J., & Wohlgemuth-Ueberwasser, C. (2015). Reconstruction of tectonic events on the northern Eurasia margin of the Arctic, from U-Pb detrital zircon provenance investigations of late Paleozoic to Mesozoic sandstones in southern Taimyr Peninsula. Geological Society of America Bulletin.